Philipps Universität Marburg

Historical solar
Analysis from
Long-term geosynchronous
Orbit

A proof of concept study to use CM SAF's MAGICSOL method to retrieve global and direct surface radiation from historical geosynchronous observations

Erstgutachter:
Prof. Dr. J. Bendix,
Philipps-Universität Marburg
bendix@staff.uni-marburg.de
+49 6421 28-24266

Zweitgutachter:
Dr. R. Müller,
Deutscher Wetterdienst
richard.mueller@dwd.de
+49 69 806 24 922

Autor:
B.Sc. Daniel Lee
Matrikelnummer: 2194295
Hauptfach: M.Sc. Environmental Geography
Nebenfach: Informatik
Lee@isi-solutions.org
+49 176 612 77269
Lutherstr. 20
61231 Bad Nauheim

Table of Contents

Index of Figures

Index of Tables

1. Introduction

The last century and the last decades in particular have been witness to dramatic, anthropogenically caused changes to the Earth's climate systems. In light of these transformations, it is increasingly important to understand our planet's energy budget. The in- and outflows of radiative energy, as well as their spatiotemporal distribution, are important for evaluating and furthering our understanding of the earth's climate (World Radiation Monitoring Center – Baseline Surface Radiation Network 2012a). They are also crucial for understanding and exploiting solar energy, which can in part be used as a mitigation strategy against anthropogenic climate change (Huld et al. 2010). Additionally, solar irradiation data can be used to better understand ecological processes (Jacobson, Seaver, and Jiashen Tang 2011) and in agricultural and hydrological applications (Otkin et al. 2005).

The Global Climate Observing System (GCOS) has identified solar irradiance, the surface radiation budget and cloud properties as essential climate variables (ECVs) (Global Climate Observing System 2012). Three factors used to measure these variables are surface incoming shortwave radiation (SIS), surface incoming direct radiation (SID) and effective cloud albedo (CAL). GCOS has called for the international exchange of historical measurements and the systematic observation of these variables in the present.

Despite the importance of these variables, current global data sets have several deficits. Ground measurement techniques are expensive and concerted efforts have failed to establish uniform measurement schemes (Hegner et al. 1998). Furthermore, due to the high spatiotemporal variability of these ECVs, a very dense network of ground stations would be necessary to generate high-quality continuous data (Hammer 2001). Model-based computations often require large amounts of input data and produce results lacking in necessary variables or with insufficient accuracy to qualify as ECVs (e.g. (Berrisford et al. 2009)). Satellite retrievals are highly accurate, but currently available data sets fail to provide all three of the above mentioned ECVs in high resolution on a global scale (R. Posselt et al. 2012).

In light of the high accuracy of satellite-based solar ECV retrievals, it is proposed that archived, historical data from geosynchronous orbit could be used to produce a global ECV data set. Some global solar irradiation data sets already exist. For example, (Lohmann et al. 2006) have used data from the International Satellite Cloud Climatology

Project (ISCCP) to retrieve surface incoming global and direct radiation on a global scale. These data, however, is reduced from the native resolution of the geostationary satellites that produced the imagery to the resolution used in ISCCP. (R. W. Mueller et al. 2009) have used Advanced Very High Resolution Radiometer (AVHRR) data collected onboard the National Oceanic and Atmospheric Association's (NOAA) Meteorological Operational satellites (MetOp) to retrieve surface incoming shortwave radiation, but using these satellites to retrieve effective cloud albedo and surface incoming direct radiation is problematic due to the low temporal resolution of the polar orbiting satellites.

In order to overcome these deficits, a new global ECV data set is need. Its data requirements should be robust enough to allow retrievals of solar direct and global irradiance, as well as cloud albedo, from a variety of different sources without needing large amounts of ancillary data, which might not be available. It should also provide data in high resolution, on a global extent and homogeneously over a period long enough for climate studies.

In this study, the feasibility of a global, high-resolution data set of surface incoming shortwave and direct radiation, as well as effective cloud albedo, is tested using the MAGICSOL method (R. Mueller, Trentmann, Stöckli, et al. 2011). The MAGICSOL method has been tested extensively and with a large degree of success for the Meteosat satellites (R. Posselt, Müller, Trentmann, et al. 2011). Because the MAGICSOL method uses a self-calibrating technique to compensate for satellite changes and sensor degradation, it is hypothesized that it will work effectively with imagery acquired onboard the GOES satellites using similar sensors to those on board the Meteosat First Generation satellites, which were used by (R. Mueller, Trentmann, Stöckli, et al. 2011) to produce the CDRs in question from Meteosat imagery. Meteosat and GOES imagery is available from the 1980s, making it possible to produce a climate-quality data set from archival data, should the method prove effective with the GOES satellites. It is furthermore proposed that using the MAGICSOL method makes it possible to produce higher quality data than is available from other sources.

In order to test this hypothesis, one month of data from all available satellites in the geo-stationary ring was used to retrieve effective cloud albedo and surface incoming shortwave and direct radiation. The data was validated using ground-based measurements with the goal of reaching the European Organisation for the Exploitation of Meteorological Satellites (EUMETSAT) Satellite Application Facility on Climate Monitoring (CM SAF) Continuous

Operations and Development Phase (CDOP) accuracy standards (R. Posselt et al. 2012). It was also compared with data produced from other sources, namely the ERA-Interim reanalysis data and the AVHRR-derived CLARA data set (see chapter 2).

Table 1.1: Accuracy targets (R. Posselt et al. 2012).

	Total shortwave radiation (W/m^2)			Direct radiation (W/m^2)		
	Threshold	Target	Optimum	Threshold	Target	Optimum
Monthly	15	10	8	20	15	12
Daily	25	20	15	30	25	20

The following chapters provide an overview of currently available data. In the following chapter, the data that was used is introduced. Following that, the MAGICSOL algorithm, as well as the validation techniques used, are explained. Thereafter, the results of the retrieval are shown and, in the next chapter, qualitatively and quantitatively validated. Finally, a discussion and conclusion compares the possibility of producing the global CDRs in question from geostationary satellites with other data sources. The study is concluded by an outlook on further possibilities for improvement and possible areas of research.

2. Current data sets and retrieval methods

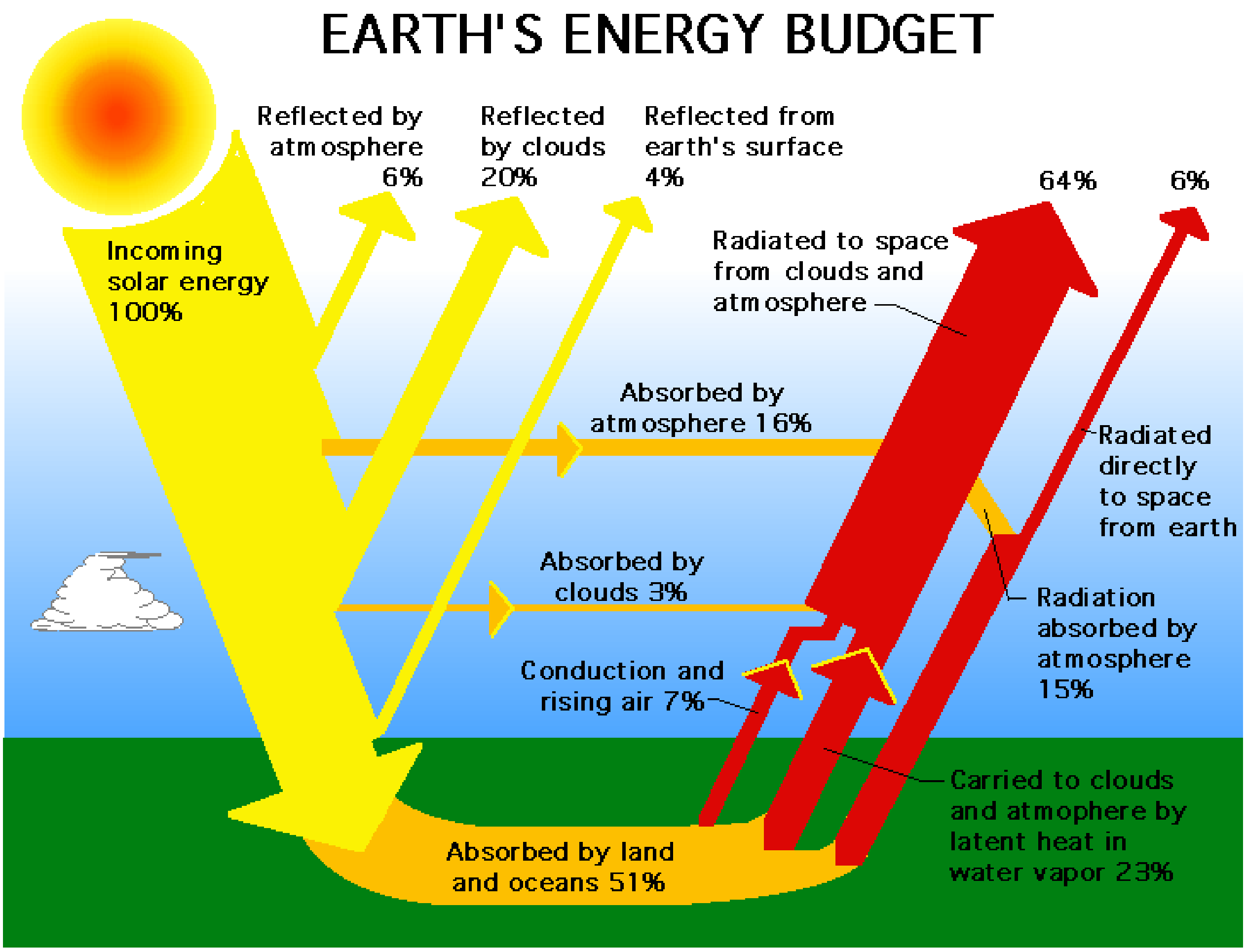

Figure 2.1: A schematic diagram of Earth's energy budget (Madigan 2011).

The main components of the earth's radiation budget are well known and the rough amounts of energy that are passed from each system component to another are fairly well understood on a global, long-term scale (see Figure 2.1). Three of the most important components are effective cloud albedo, surface incoming solar radiation and surface incoming direct radiation (see Figure 2.2). These essential climate variables are the focus of this study.

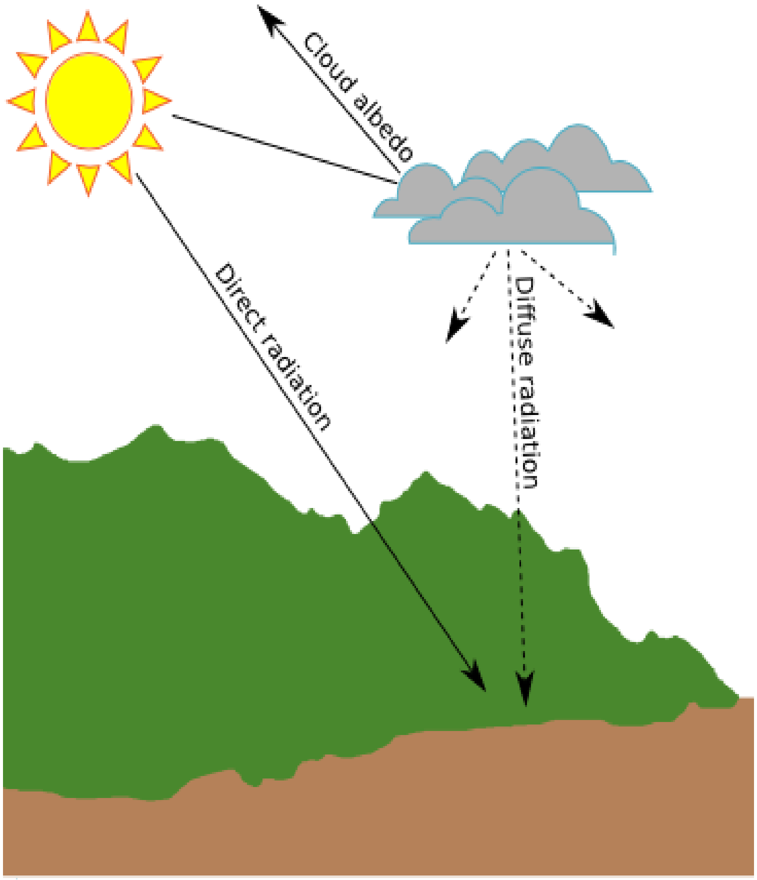

Figure 2.2: The essential climate variables examined in this study. Total shortwave radiation is the sum of diffuse and direct radiation. Modified by author, based on: (Department of Primary Industries, State Government of Victoria 2011).

Each of these ECVs is tied closely not only to cloud cover, but also to cloud types (Deneke, Feijt, and Roebeling 2008). This makes them highly spatially variable, as not only the latitude and season, but also clouds strongly influence them (see Figure 2.3). The ECVs are not only spatially, but also temporally highly variable - (Lohmann et al. 2006) showed that the solar irradiation is highly variable in time as well, so that long time series are necessary in order to accurately describe the amount of radiation that should be expected at a given location (see Figure 2.4).

Great uncertainties still exist concerning solar irradiation and cloud albedo over the world's oceans (R. Mueller, Trentmann, Träger-Chatterjee, et al. 2011). As these areas make up most of the earth's surface, understanding their contributions to the global radiation budget are crucial to quantifying past and predicting future climate change (United Nations 2007).

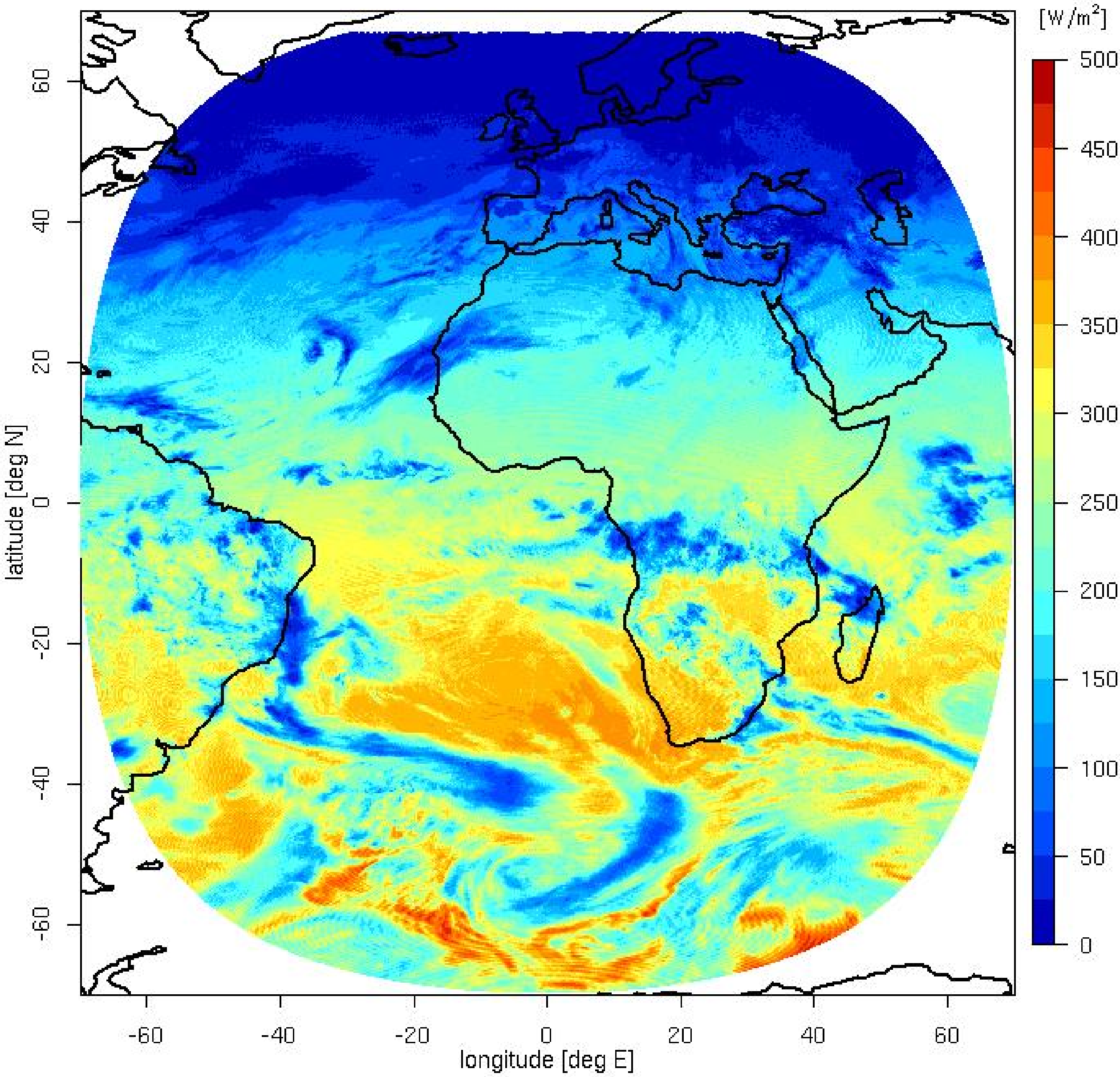

Figure 2.3: Daily average of total surface incoming shortwave radiation on January 1 1983, derived from Meteosat First Generation imagery. Total surface incoming radiation is the least variable of the three ECVs in this study and is nonetheless highly variable, not only longitudinally but also on other scales (R. Posselt, Müller, Stöckli, et al. 2011).

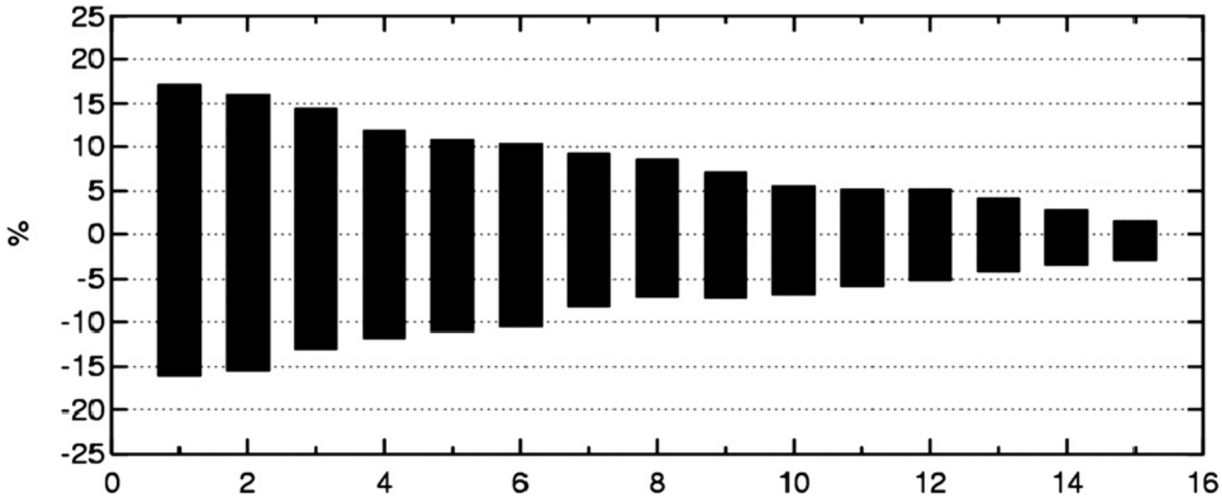

Figure 2.4: Minimum & maximum deviations from 18 year mean when averaging over limited time spans. The x axis descrbes the number of years used to produce an average, the y axis the deviations from the 18 year mean. Using time series with less than seven years results in deviations from the 18 year mean of more than 10% (Lohmann et al. 2006).

In the following sections, relevant current measuring techniques are introduced, as well as available data sets with their respective advantages and disadvantages.

2.1. Ground based data

Ground-based data have several advantages compared to other types of data. The measurements are performed directly, rather than being derived as secondary data, and the instrument calibration can be tested if needed. For this reason, ground-based measurements are often considered to be ground truth and are used for validation when testing other measurement techniques.

There are several drawbacks associated with ground-based measurements. As with almost every type of ground-based measurement, the instruments needed to measure solar global and direct irradiation only provide information about the point at which the measurement took place, so that it is difficult to use them for applications that require spatially continuous data. Cloud albedo cannot be measured from the ground directly, and the instruments necessary to measure solar global and direct irradiation are expensive compared to other meteorological instruments (e.g. (Omni Instruments 2012)). Because careful calibration and frequent maintenance for the instruments is required, it would be prohibitively expensive to establish a dense, widespread network of ground stations. (Bureau of Meteorology, Commonwealth of Australia 2012).

Despite these disadvantages, ground stations are an important and necessary part of the global infrastructure needed to observe solar ECVs due to their role as providers of ground truth data.

2.1.1. Measurement techniques

Because the ECV cloud albedo refers to the reflection of sunlight from clouds into space without striking the earth, there is no way to measure it directly from the ground. Both solar global irradiation and solar direct irradiation can, however, be measured using ground-based instruments.

Figure 2.5: A research-grade pyranometer (Wikimedia Commons 2012b).

Figure 2.6: A research-grade pyrheliometer (Wikimedia Commons 2012a).

Global irradiation is measured on a horizontal surface using pyranometers. Pyranometers operate by measuring changes in temperature on a black surface using thermocouples. In order to insulate the sensing element from non-radiative temperature changes, the sensor is shielded by two glass domes (see Figure 2.5). When radiation strikes the pyranometer's sensing element, it produces heat, which flows into the cooler pyranometer body. The temperature difference between these two elements creates an electromotive force which is measured and recorded as an indicator of the level of irradiance occurring at a given point in time (Bureau of Meteorology, Commonwealth of Australia 2012).

Global irradiation measurements with pyranometers are subject to various errors. The degree to which the sensing element is heated is dependent on the conversion of radiative into thermal energy. The energy is absorbed by a black paint on the sensing element, which should optimally absorb all wavelengths equally. However, as the paint degrades over time, this can change, so that certain wavelengths are absorbed less effectively. This decreases the total amount of irradiation measured (Bureau of Meteorology, Commonwealth of Australia 2012). As the sensor degradation is a result of many processes, it must be compensated by recalibrating the device. There are many methods to do this, and all of them require a high degree of knowledge about calibration techniques and direct work with the individual device (Reda, Stoffel, and Myers 2003).

Further limitations are posed by the device design itself. The absorptance ratio of the sensing element decreases as the solar incident angle increases. As pyranometers measure irradiation on a horizontal surface, the irradiation at low solar altitudes is measured with a negative bias (Bureau of Meteorology, Commonwealth of Australia 2012). Furthermore, the insulating domes protecting the sensing element from unwanted temperature changes are composed of glass which both reflects and absorbs radiation. Thus, the insulators both prevent some radiation from reaching the sensor, while also exchanging radiation with the sensor itself. Additionally, dust or other obstructions on the insulating dome affect the amount of irradiation observed by the pyranometer (Srivastava 2009).

Solar direct irradiation is more difficult to measure than solar global irradiation due to the fact that measuring direct irradiation requires that only the radiation traveling directly between the sun and the measuring instrument be measured. It is measured as the solar energy reaching a plane perpendicular to the sun's direct beam on the earth's surface. This is accomplished by using pyrheliometers with a viewing angle of 5° (see Figure 2.6). The pyrheliometer must be mounted on a solar tracker to ensure that it is continuously pointed at the sun (Bureau of Meteorology, Commonwealth of Australia 2012).

Field pryheliometers operate according to the same principle as pyranometers and are thus subject to most of the same errors. Pyrheliometer calibration even more labor intensive than pyranometer calibration, requiring two to three days of testing. Each day, 100 one-minute measurements are compared between the field pyrheliometer and a stable, self calibrating cavity radiometer (Flowers 1978).

2.1.2. Data sets

High-quality ground-based solar measurements are hard to obtain. Most databases are comprised of collections of measurements gathered at single stations at single points. Few contain uniform data, so that the data from many stations is often restricted to only global irradiation.

Noteworthy point databases include the National Solar Radiation Data Base from the U.S. Department of Energy's National Renewable Energy Laboratory, which comprises hourly measurements of global irradiation collected at 237 stations from 1961-1990 and measurements of solar global and direct irradiation collected at 1,454 stations from 1991-2005 (U.S. Department of Energy, Office of Energy Efficiency and Renewable Energy, National Renewable Energy Laboratory 2008). The National Solar Radiation Data Base is free to use for any purposes, but is only available for the United States.

The European Solar Radiation Atlas (ESRA) contains station measurements collected across Europe from 1981-1990 by the World Radiation Data Centre (WRDC) and various other institutions (Page et al. 2001). These measurements were conducted in varying degrees of quality – monthly averages of global irradiation are available from 586 stations, whereas daily sums of global irradiation are only available from 90 stations. Six stations provide daily solar direct irradiation values. The data are also available as spatially continuous monthly average rasters and one yearly average raster with a resolution of approximately 10 km. These were computed by interpolating the monthly averages of solar global and direct irradiation from all stations. At stations where direct irradiation was not measured, it was computed using empirical formulas. The raster data is rated with an uncertainty of 25 Wh/m^2 (Scharmer and Greif 2000), well below the CM SAF quality threshold used in this study (R. Posselt et al. 2012).

Another spatially continuous solar data set created from ground measurements is the Joint Research Centre's Photovoltaic Geographical Information System (PVGIS). PVGIS-3 was created by using spline interpolation on the monthly station measurements contained in the ESRA database and contains monthly averages of solar global and direct irradiation for all of Europe with a resolution of 1 km. Linke turbidity maps were used to help estimate the composition of global irradiation in diffuse and direct irradiation (Huld et al. 2010). Satellite data from the HelioClim project (described in chapter 2.3.2) were used for the Mediterranean Basin, Africa and southwest Asia (Huld and Dunlop 2012a). In validation tests, the PVGIS-1 database has a similar root mean square error as the ESRA database, with better performance in winter. This is most likely due to the fact that PVGIS also considers shadowing effects, which were not used for the ESRA database (Huld and Dunlop 2012b). It should be noted that the new version of PVGIS, PVGIS-4, now uses satellite data rather than station measurements due to the higher data quality and the increased ease in keeping the database current (Huld and Dunlop 2010, 2010).

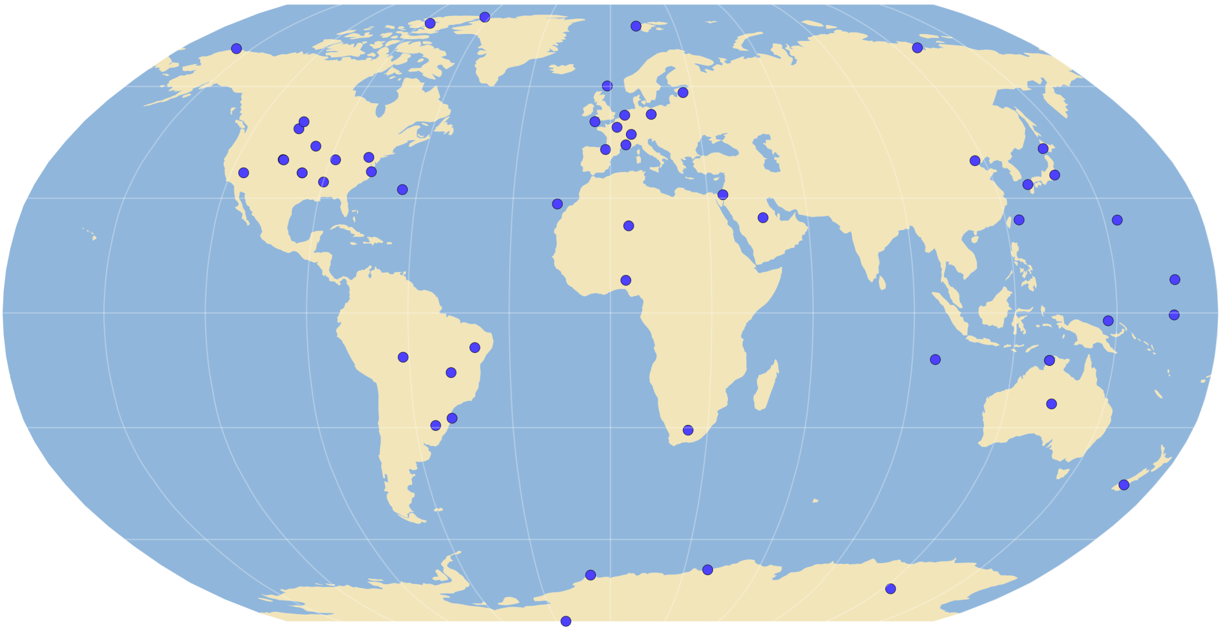

Figure 2.7: BSRN stations currently in operation. Based on: (Ohmura et al. 1998).

The Baseline Surface Radiation Network (BSRN) is a high quality radiation monitoring network operated by the World Climate Research Programme (WCRP) as part of the Global Energy and Water Cycle Experiment (GEWEX) (World Radiation Monitoring Center – Baseline Surface Radiation Network 2012a). It is comprised of 56 ground measuring stations distributed throughout the world (see Figure 2.7). The measurements are centrally archived at the World Radiation Monitoring Center and subjected to exhaustive quality controls (Hegner et al. 1998). Each station takes several essential measurements of radiation, synoptic weather and the upper atmosphere. These essential measurements include solar global and direct irradiation. Additionally, many stations measure expanded variables (World Radiation Monitoring Center – Baseline Surface Radiation Network 2012b). The BSRN is considered one of the highest quality, global available, research-grade radiation networks.

2.2. Reanalysis data

Reanalysis data is produced by assimilating past observed data into complex, predictive weather models. The large amount of available historical data can be modeled using a unified modeling scheme, producing consistent outputs of several variables that cannot be measured directly over a long period of time. This makes it possible to effectually simulate data for a point of time that is already past that was not or could not be measured.

Reanalysis offers many possibilities in the context of cloud albedo and solar irradiation, especially as opposed to operational numerical weather prediction. Because a single model is used over a long time period, no inhomogeneities are introduced into the output data through changes in the model or the data assimilation scheme. Additionally, data can be produced that extends far into the past rather than only into the near future.

However, as with all modeling applications, reanalysis is subject to uncertainties. For example, each model step is only as good as the data it is given. This means that low data quality, due to poor instrument setup, degraded instruments, instrument changes or the like, leads to poorer results. The model skill is also of concern – uncertainties in the model are propagated into the output data.

Reanalysis is also very computationally expensive, as it requires the use of a dynamic circulation model. It also requires large amounts of input data. The high computational costs and low data input density lead necessarily to low resolution outputs, making it difficult to utilize reanalysis data in regional or local applications.

In principle, reanalysis data could be produced using regional climate models for single regions and smaller areas, but in practice most reanalysis data is made using general circulation models on a global scale. In the following sections, some of the main tenents of these models are briefly described, as well as relevant global data sets.

2.2.1. Computation techniques

An extended discussion of circulation modeling techniques would go beyond the scope of this study. For additional information on general circulation models and numerical weather modeling in general, see e.g. (Satoh 2004) or (Warner 2011).

For the scope of this study, it should suffice to say that numerical weather models simulate complex exchanges in pressure, air mass, temperature, moisture, etc. The level of complexity is limited only by the developers' understanding of the modeled systems and the available data. For example, drag, albedo and moisture exchange of the earth's surface can be simulated in circulation models and, if desired, they can be coupled with e.g. ocean models to more accurately model exchanges of heat, moisture and materials with the ocean, as well as with regional climate models to more accurately model regional scale occurrences.

Generally, cloud albedo is not included as an explicit output in reanalysis data sets. Downward solar global and (sometimes) direct irradiation is most often modeled by computing the transmittance and refractive properties of the simulated atmospheric column (e.g. (Matricardi et al. 2004)).

2.2.2. Data sets

Due to the high amount of computing power required to produce reanalysis data, only agencies with large institutional capacity are able to produce them. Some of these data are only available for certain spatial domains. For an up-to-date systematic comparison of most available reanalysis data sets, including those with a limited spatial domain, see (Reanalysis Intercomparison and Observations 2012). Due to the global nature of this study, only global data sets will be introduced in this section.

The Japanese 25-year Reanalysis (JRA-25), produced by the Japanese Meteorological Agency (JMA) and the Central Research Institute of Electric Power Industry (CRIEPI), is available for the years 1979-2004 and is continued into the present through the JMA Climate Data Assimilation System (JCDAS). Its primary data source is from satellites, using geostationary observations to compute wind vectors and retrieving brightness temperatures from the TIROS Operational Vertical Sounder (TOVS). Precipitable water and other data are adjusted according to satellite and ground-based observations using a three-dimensional variational method (3D-Var). All fields are provided with a resolution of 1.25° on a 6-hourly basis. Surface solar global irradiation is included among the output data (Onogi et al. 2007, -25).

The National Centers for Environmental Prediction (NCEP) and National Center for Atmospheric Research (NCAR) have produced several reanalysis data sets, including the NCEP/NCAR Reanalysis I (R1). This data set provides 6-hourly outputs which include surface solar global and direct irradiation (US Department of Commerce 2008). Several data sources were assimilated for the reanalysis, including measurements conducted on ships, airplanes, radiosondes, ground stations and satellites. The initial input data is quality controlled and is extended into the future with a horizontal resolution of 2.5° (Kalnay et al. 1996).

The National Aeronautics and Space Administration (NASA) also maintains a reanalysis data set comprised of data from 1979 to the present. Titled Modern Era Retrospective-Analysis for Research and Applications (MERRA), the reanalysis data is produced using mthe Goddard Earth Observing System (GEOS-5) Atmospheric General Circulation Model (AGCM). The data set has the highest resolution among global reanalysis data sets (0.6°

longitude x 0.5° latitude) (Rienecker et al. 2011). Surface solar global irradiation is computed with consideration of simulated absorption and scattering from water vapor, ozone, oxygen, carbon dioxide, clouds and aerosols (Chou and Suarez 1999).

In Europe, the European Centre for Medium-Range Weather Forecasts (ECMWF) produces reanalysis data as a part of the ERA (ECMWF Reanalysis) project. The ERA-Interim data set provides surface solar global irradiation at 6-hour intervals (European Centre for Medium-Range Weather Forecasts 2012). Observational data from ground stations and satellites, both geosynchronous and polar-orbiting, is assimilated into the reanalysis using a four-dimensional variational (4D-Var) analysis scheme encompassing data from 1979 to the present with plans to eventually cover the entire 20th century (Dee et al. 2011). Irradiation is simulated using a fast radiative transfer model, Radiative Transfer for the Television Infrared Observation Satellite (TIROS) Operational Vertical Sounder (RTTOV). The model computes aerosol optical depth from the model's simulated temperature, water vapor, ozone and surface emissivity (Matricardi et al. 2004). The data is available in a user-specified resolution up to a resolution of 0.75° (Uppala et al. 2005).

All of the listed reanalysis data sets are considered to have a high quality and their global coverage is quite useful in many applications. However, the data is subject to the compound weaknesses of the data ingested and the models used, which should always be used with caution. Additionally, their low spatial resolution limits their usage to global applications, making them unable to meet the requirements for global ECV data sets outlined in chapter 1.

2.3. Satellite based data

Satellites observe the earth using electromagnetic radiation. They can be seen as a mixture between direct measurements, using ground-based instrumentation, and more abstractly derived data, such as reanalysis data. Because satellites are only able to directly observe the radiance of a given area in their field of view, climate variables have to be computed indirectly in order to retrieve them from satellite data using models. These models are most often several orders of magnitude simpler than the weather models used to produce reanalysis data and require less data to run.

Obtaining climate data from satellite observations has several advantages. Unlike reanalysis data, which is computed indirectly using several simulated variables, satellite data often has a more immediate relationship to observational data. This reduces the risk of compound errors producing biased data. And in contrast with ground-based measurements, satellites make spatially continuous measurements, eliminating the need for modeling or interpolation to fill spatial gaps in data sets. Additionally, a single instrument can be used to image large portions of the earth's atmosphere or surface, reducing the uncertainty caused by using measurements from several different instruments that may or may not be properly intercalibrated.

One would be mistaken, however, to attempt to use satellite data as a sole data source. Satellites cannot reach the temporal resolution of high-quality ground-based instruments, because the satellites are constantly in motion. Polar orbiters rotate the earth around the poles and can need days to image the same portion of the earth's surface twice. This disadvantage is compensated in part by their higher resolution – their low orbit allows them to sacrifice a wide viewing angle for a higher spatial resolution. Geosynchronous satellites maintain a stable position above a point on the equator and thus can image more frequently, but in order to keep station they have to orbit farther away than polar orbiters, thus lowering their spatial resolution. Geosynchronous satellites have the advantage that they can image their entire field of view in an hour or less, although not all satellites work with this schedule. Additionally, climate variables derived from satellite observations should be validated using ground-based data to the extent possible in order to verify that the sensor on board the satellite and the model used to compute the variable are functioning correctly.

Despite these disadvantages, the advantages of satellite data greatly outweigh their advantages. The spatial resolution is sufficient for mesoscale applications and the spatially continuous measurements validate better than data interpolated between stations. Also, because they are above clouds, they are able to measure cloud albedo more directly than any other technique. These are the reasons that satellites were chosen as the data source of choice for this study.

2.3.1. Retrieval techniques

Satellites observe climate variables by examining electromagnetic radiation that is emitted by or reflected from the earth and the atmosphere. This presents several difficulties when attempting to measure solar irradiation at the earth's surface, as well as when measuring cloud albedo. In order to overcome these shortcomings, models of varying complexity must be used in order to compute the amount of radiation reaching the earth's surface and the amount reflected by clouds.

The basic principle behind all satellite-based surface irradiation retrievals is that the atmosphere affects the amount of radiation reaching the earth's surface. The most important factor in this equation, and the most easily observable one from space, is cloud cover. In the short wavelengths relevant for solar surface global and direct irradiation, clouds reflect and absorb radiation from the sun, reducing the amount of radiation reaching the surface and obscuring it from the satellite's view while increasing the albedo of the point observed.

Several techniques exist to use satellite data to retrieve solar irradiation. Already in 1982, (Diak, Gautier, and Masse 1982) used an energy balance model to produce monthly maps of total surface global irradiation on a 12 x 12 km grid using data from the Geostationary Operational Environmental Satellites (GOES). The results were judged to be comparable to interpolated ground measurements. More than a decade later, (Diak, Bland, and Mecikaski 1996) used the second generation of GOES to produce daily global irradiation values using a simple radiative transfer model and an albedo based cloud detection scheme.

Modern satellite retrievals compare several observations of the same location on the earth's surface under the assumption that at some point the point will have been observed under clear sky conditions. The observation with the lowest reflectance is assumed to be cloud-free, with higher reflectances being attributed to cloud reflectance (e.g. (Diak, Bland, and Mecikaski 1996)). This basic retrieval principle can be expanded upon by assimilating additional data concerning the atmosphere, including but not limited to the elevation-based air mass (P. Ineichen and Perez 1999), atmospheric observations conducted by other sensors or satellites, satellite-derived cloud microphysical properties (Deneke, Feijt, and Roebeling 2008), ground-based measurements and circulation model outputs (Gupta et al. 2010).

This simple principle, however, is not enough alone to compute solar irradiation at the earth's surface. Not only clouds affect the reflectance observed at a single location, but also the land cover. Additionally, the observational geometry – sun height, the satellite's observation angle, etc. – affects the perceived brightness of a given point. These factors must be accounted for and, where necessary, corrected using observational data. Normalizing satellite counts based on solar geometry can be solved with relative ease, as the positions of the sun, the earth and the satellite during each observation are known

(Cano et al. 1986). Changes to the earth's surface reflectance, however, are more difficult to detect. Highly reflective areas, such as deserts or regions covered in ice or snow, present special difficulties. Several algorithms exist to differentiate between snow and clouds by e.g. classifying pixels depending on their spectral characteristics (Gesell 1989) or their temporal evolution (R. Posselt et al. 2012). Deserts continue to present problems due to their stable, high albedo.

After having detected the degree of cloud cover and any additional variables used by the algorithm, it is possible to compute the amount of solar irradiation at the earth's surface. Most algorithms employ two models for this step: one for clear skies and one for cloudy skies. The model outputs are varied – some produce only values concerning solar global irradiation, while others also account for direct irradiation. Some even produce spectrally resolved irradiation values (R. Mueller et al. 2012).

Although cloud albedo can be more easily computed than surface irradiation, most algorithms neglect this important climate variable. It can be computed by observing changes in pixel brightness over a period of time and examining the brightness offset compared to the minimum observed brightness (Hammer 2001). The cloud albedo can then be computed by normalizing the brightness counts according to the solar elevation, which has a daily and an annual cycle, and the sun-earth distance, which varies seasonally. Additional reflectance above the minimum observed brightness is considered a product of Lambertian reflection by clouds (R. Mueller, Trentmann, Stöckli, et al. 2011).

In principle, all of these retrieval techniques are possible using any satellite with the correct sensors, whether the satellite orbits the poles or maintains a geosynchronous orbit. Both configurations have advantages and disadvantages. Polar orbiters generally have a higher spatial resolution due to their closer proximity to the earth, but they only observe a single swatch of the earth's surface at a time and it can take up to several weeks for a satellite to return to observe the same location. This makes it difficult to reach a high level of accuracy, especially concerning cloud albedo and direct irradiation, in light of the high temporal variability of cloud cover, which has a strong influence on the three ECVs that are the focus of this study and the two mentioned ECVs in particular. Although geo-synchronous satellites observe the earth from a much greater distance, they observe the same point on the earth's surface several times on the same day. Additionally, their resolution of down to one kilometer at nadir makes them well-suited for climate studies, which focus more on regional and global rather than local scales. One large drawback of working exclusively with geosynchronous satellites, however, is that due to their viewing geometry they cannot observe the earth's poles. In order to obtain satellite observations of high latitudes, it is therefore necessary to use polar-orbiting satellites.

2.3.2. Data sets

There are only few data sets that provide information on cloud albedo. In contrast, there is an ever-growing number of satellite-derived data sets concerning surface solar irradiation. In the following section, the focus will be on data sets that come close to satisfying the requirements of this study.

NASA and the Global Energy and Water Cycle Experiment (GEWEX) have used data collected during in the International Satellite Cloud Climatology Project (ISCCP) to produce a Surface Radiation Budget (SRB) product, which provides solar global and direct irradiation values for the entire earth from 1993 to 2007 on a 1x1° grid. The data was creating using a modified version of the method by (Pinker and Laszlo 1992), which uses a radiative transfer model and modeled water vapor and temperature column values taken from the GEOS-4 model results, model-derived aerosol climatologies, satellite observations of the ozone column and satellite observations of cloud cover to calculate downwelling solar global and direct irradiation. Although this data is conveniently available for the entire globe, it has a very low resolution. Also, the bias as compared to BSRN measurements is well above the target bias values set for this study (Stackhouse 2011).

The method used to produce the SRB product was later improved by (D. P. Kratz et al. 2012) and used in the Fast Longwave And Shortwave Radiative Fluxes (FLASHFlux) project to produce near real-time radiation data. FLASHFlux uses data collected by the Terra and Aqua satellites, as well as ouputs produced by the GEOS 5 general circulation model. The FLASHFlux product utilizes the Langley Parameterized Shortwave Algorithm (Gupta et al. 2010) to produce data on solar global irradiation within a week of observation. Its aim is to provide near real-time irradiation data until more accurate irradiation data is available from the Clouds and the Earth's Radiant Energy System (CERES) sensor, which is published 6-12 months after the point of observation (Sawaengphotkhai 2009).

NASA's CERES sensors have been used to provide data collected onboard polar orbiting satellites since 1998. It utilizes data observed by CERES, as well as model outputs and surface observational data to compute monthly surface fluxes and other variables on a 1° global grid (Wielicki et al. 1996). It is considered more accurate than the SRB and

FLASHFlux products, but only rarely meets the quality standards set for this study (David P. Kratz et al. 2010). Additionally, the spatiotemporal resolution does not meet this study's requirements.

The HelioClim databases contain data observed by the Meteosat Prime satellite (see chapter 3.1). They were produced using the Heliosat-2 method (Rigollier, LefÈvre, and Wald 2004, -2), which is based on the Heliosat-1 method by (Cano et al. 1986). They provide daily means of solar global surface irradiation from 1985-2005 from Meteosat observations, collected in reduced resolution (~20 km) during the ISCCP project (Lefèvre, Wald, and Diabaté 2007, 2). Additionally, hourly averages of solar surface global irradiation are available from 2004 onwards with a resolution of approximately 10 km using the Helisat-2 method (Rigollier, LefÈvre, and Wald 2004, -2). The data covers the field of view of Meteosat Prime and the low-resolution version covering the time from 1985 to 2005 are available for free, with high-resolution, more current data available for a fee from the Solar Radiation Data (SoDa) platform (SoDa: Solar Radiation Data 2012).

The SolarGIS database contains 30 minute averages of surface solar global and direct irradiation observed at the Meteosat-Prime, Meteosat-IODC, GOES-East and GMS positions with a resolution of approximately 250 m. Meteosat-Prime coverage is available from 1994 to present, Meteosat-IODC and GOES-East data is available since 1999 and GMS coverage from 2005. The satellite observations are combined with gridded air temperature at 2 m height and water vapor data from NCEP, atmospheric optical depth calculated from data provided by ECMWF and snow depth data provided by NOAA (GeoModel Solar s.r.o. 2012b). The data validates well compared with other commercial data sets (Pierre Ineichen 2011), but is only available for very high prices (GeoModel Solar s.r.o. 2012a).

(Zhang et al. 2004) have used ISCCP data collected from all geosynchronous satellites in combination with NASA's Goddard Institute for Space Studies (GISS) radiative transfer model (Bishop, Rossow, and Dutton 1997) and additional ancillary data to produce a data set of surface global irradiation spanning the years 1983 to 2001. The data is available in three hourly time steps with a resolution of 280 km. The data set is long enough for use in climate studies, but with a much too low resolution and few possibilities to continue producing it into the future.

The CM-SAF CLoud And Radiation project (CLARA) provides daily averages of surface solar global irradiation data for the entire world using AVHRR observations collected on polar orbiting satellite platforms for the entire globe from 1989 to 2009 on a 0.25° x 0.25° grid (Trentmann, Müller, et al. 2012a). It incorporates ancillary data from the ERA-Interim data set, aerosol information from the GADS/OPAC data base and surface albedo from the SARB/CERES project and utilizes the methodology outlined in (R. W. Mueller et al. 2009) to compute global irradiation. The CLARA data set validates quite well (Trentmann, Müller, et al. 2012b), but it provides only data concerning one of the three CDRs focused on in this study at relatively low resolution.

The data that most closely matches the goals of this study are the CM SAF Meteosat (MVIRI) Solar Surface Irradiance and effective Cloud Albedo Climate Data Sets. They provide all three of the goal variables for the Meteosat full disk in Meteosat First Generation native resolution (0.3° x 0.3°) as hourly means from 1983 until the introduction of Meteosat Second Generation in 2005 (Trentmann, Träger-Chatterjee, et al. 2012) with the method described in (R. W. Mueller et al. 2009), which requires only observations from the visual channel and readily available water vapor, ozone and aerosol climatologies. This data set is being continually extended using current data using Meteosat Second Generation satellites (Trentmann et al. 2010). These data have been validated to have the highest accuracy among other publicly available, global data sets (R. Posselt et al. 2012). Through the availability of all three goal variables, the data's high accuracy and resolution and the presence of a long time series, these data fulfill the requirements for the current study, but only for the field of view of the Meteosat First Generation satellites. Due to MAGICSOL's low data requirements and its self-calibration mechanism, it should be possible to apply it to observations from sensors on board other satellite platforms (e.g. GOES and GMS) (R. Posselt, Müller, Trentmann, et al. 2011). The plausibility of extending these data to the other satellites in the geostationary ring will be the focus of this thesis' empirical work.

3. Data

As is shown in chapter 2, few data sets are available containing data on cloud albedo. Among the many available data sets concerning surface solar global and direct irradiation, none fulfill all criteria outlined in chapter 1: open availability, high resolution, long-term availability and high accuracy.

In the following sections, the data used in this study in order to fill these gaps will be introduced.

3.1. Satellite data

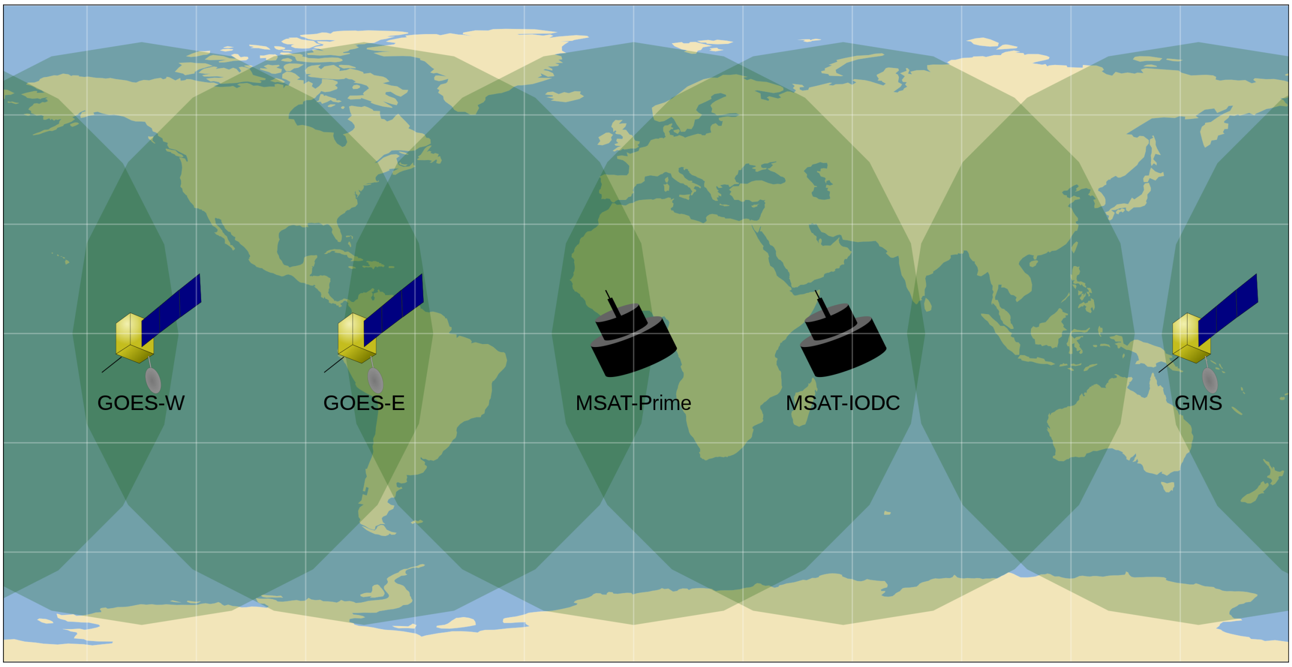

Figure 3.1: Satellite spatial coverage and satellite positions. Based on: (NOAA US Department of Commerce 2012a; EUMETSAT 2012).

Geosynchronous satellite coverage has been available for certain parts of the world since the 1970s. By 1998, coverage of the Indian Ocean was added, closing the last spatial gaps in geosynchronous satellite coverage. The geosynchronous satellites have been swapped out frequently, but attempts have been made to occupy the same positions consistently, providing comparable observations over a long time series (see Figure 3.1).

Because the focus of this study is to prove the feasibility of a global CDR data set, not all of the available data is relevant. During long periods of time, the GOES satellites switched frequently between the GOES-W and the GOES-E positions, causing difficulties with the data and making these periods less useful for our current goal. Before 1998, the Meteosat-IODC (Indian Ocean Data Coverage) position was not occupied, meaning that it would be better to use data from after this date. Also, acquiring data from the JMA has proven difficult, so that time frame was desirable where coverage from the GMS position was provided by either EUMETSAT or NOAA. From 4/23/2003 – 7/13/2004, normal coverage was provided at the GOES-W and GOES-E positions by GOES-10 and GOES-12, respectively, and due to technical problems with JMA's GMS-5 satellite, the decomissioned GOES-9 satellite was recommissioned to provide temporary on-site service from the GMS position until the next JMA satellite, MTSAT, was launched (Morris 2012). During the same time, normal Meteosat coverage by EUMETSAT was provided by Meteosat-7 at the

Meteosat Prime position and Meteosat-5 at the Meteosat-IODC position (EUMETSAT 2012). This provided full geosynchronous coverage of the entire planet, excepting the poles, with all data readily available from EUMETSAT and NOAA. One month, June 2003, was chosen from this test period for use in this feasibility study.

For a more detailed description of when each satellite position was occupied by what satellite, see Table 3.1.

Table 3.1: Temporal coverage for each satellite position. Data that are unavailable for this study are shown in gray: GMS due to data acquisition difficulties, GOES-6 and -7 because of difficulties associated with their variable positions, and Meteosat Second Generation because it is currently being used to produce the ECVs of this study using another method and is therefore not relevant for the study's goal of producing data from archived observations. Sources: (EUMETSAT 2012; NOAA US Department of Commerce 2012a; Japanese Meteorological Agency 2012).

<table>
<tr><th>Year</th><th>GOES-W (-135°)</th><th>GOES-E (-74°)</th><th>MSAT-Prime (0°)</th><th>MSAT-IODC (57.5°)</th><th>GMS (155°)</th></tr>
<tr><td rowspan="3">1978 – 1980</td><td>GOES-2</td><td>SMS-1</td><td rowspan="2">Meteosat-1</td><td rowspan="13"></td><td></td></tr>
<tr><td rowspan="2">GOES-3</td><td rowspan="2">SMS-2+</td><td rowspan="3">GMS</td></tr>
<tr><td></td></tr>
<tr><td rowspan="4">1981 – 1985</td><td rowspan="2">GOES-4</td><td rowspan="3">GOES-5</td><td rowspan="5">Meteosat-2</td></tr>
<tr><td rowspan="2">GMS-2</td></tr>
<tr><td rowspan="7">Variable – GOES-6 & GOES-7</td></tr>
<tr><td rowspan="5">Variable – GOES-6 & GOES-7</td><td rowspan="3">GMS-3</td></tr>
<tr><td rowspan="3">1986 – 1990</td></tr>
<tr><td>Meteosat-3</td></tr>
<tr><td>Meteosat-4</td><td rowspan="3">GMS-4</td></tr>
<tr><td rowspan="2">1991 – 1995</td><td rowspan="2">Meteosat-5</td></tr>
<tr><td rowspan="4">GOES-8</td></tr>
<tr><td rowspan="2">1996 – 2000</td><td>GOES-9</td><td>Meteosat-6</td><td rowspan="3">GMS-5</td></tr>
<tr><td rowspan="5">GOES-10</td><td rowspan="5">Meteosat-7</td><td rowspan="5">Meteosat-5</td></tr>
<tr><td rowspan="3">2001 – 2005</td></tr>
<tr><td rowspan="4">GOES-12</td><td>GOES-9++</td></tr>
<tr><td rowspan="6">MTSAT</td></tr>
<tr><td rowspan="3">2006 – 2010</td></tr>
<tr><td rowspan="3">GOES-11</td><td rowspan="4">Meteosat Second Generation</td><td rowspan="4">Meteosat-7</td></tr>
<tr><td rowspan="3">GOES-13</td></tr>
<tr><td rowspan="2">2011 – 2012</td></tr>
<tr><td>GOES-15</td></tr>
</table>

Although the GOES and Meteosat satellite series can be considered to be quite similar, there are some differences that need noting. The Meteosat Visible and InfraRed Imager (MVIRI) instrument on board the Meteosat platform scans with a ground resolution of 2.5 km at nadir, whereas the GOES imager has a nadir resolution of 1 km and GMS a resolution of 1.25 km. The imagers' visual channels also have different response spectra – Meteosat's visual band observes electromagnetic radiation with wavelengths from 0.5 – 0.9µm, while GOES observes from 0.5 – 0.7µm. The GMS visual band is similar to that of Meteosat, extending from 0.55 – 0.9µm (NOAA US Department of Commerce 2003). The extent to which this affects the accuracy of the algorithm used in this study will be evaluated during the validation process (see chapter 4).

Because June of 2003 was used, no GMS data was obtained for this study. Raw data for processing was obtained for the GOES-W, GOES-E and GMS positions directly from the NOAA Comprehensive Large Array-data Stewardship System (CLASS) archive in the netCDF format (NOAA US Department of Commerce 2012b). Preprocessed data containing the surface solar global and direct irradiation, as well as cloud albedo, for the Meteosat Prime position was provided by the EUMETSAT Satellite Application Facility on Climate Monitoring in the netCDF format (EUMETSAT Satellite Application Facility on Climate Monitoring 2012) and for the Meteosat-IODC position by the PVGIS project as a GRASS GIS database (European Union 2012). The total amount of data collected amounted to 4 terabytes.

3.2. Climatologies

The MAGICSOL method, which was used in this study to compute the goal CDRs, uses aerosol, water vapor and ozone climatologies in addition to satellite observations to provide additional data concerning the atmosphere for its radiative transfer model (RTM) (R. Mueller, Trentmann, Stöckli, et al. 2011).

The aerosol climatologies are based on medians from the AeroCom model and AERONET ground measurements on a 1x1° grid (Kinne et al. 2006). These climatologies validate quite well in comparison with similar data sets, such as those offered by NCEP, when evaluating surface solar global irradiation. This is particularly true for areas with few measurements, which are of especial interest in this study (Pierre Ineichen 2010).

Water vapor climatologies were taken from the global reanalysis data set by ECMWF (ERA-40 for years before 1989 (Uppala et al. 2005) and ERA-Interim from 1989 onwards (Berrisford et al. 2009)). In order to reduce the amount of input data required, monthly values of the total water vapor column were interpolated onto a 0.5x0.5° grid (R. Mueller, Trentmann, Träger-Chatterjee, et al. 2011).

The ozone input into the RTM was based on ozone content of the standard atmosphere by (Krämer et al. 2003).

3.3. Validation data

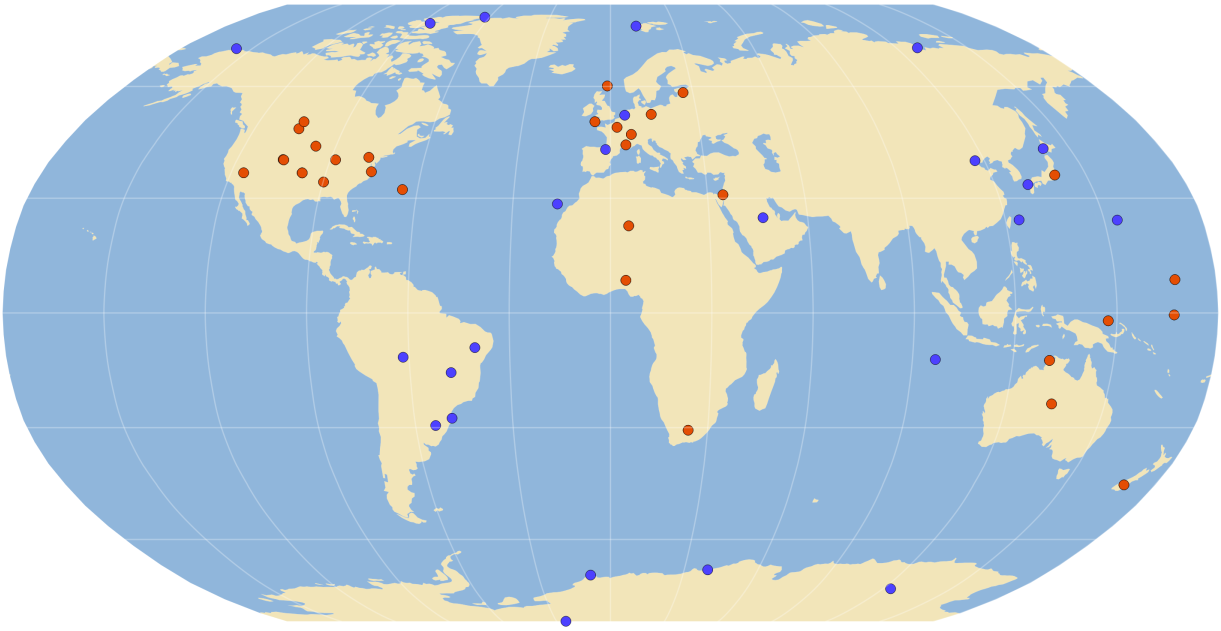

Figure 3.2: BSRN stations. Stations that registered measurements during the time period of this study are in red, other stations without reported data for June 2003 or outside the used satellites' fields of view are in blue. Based on: (Ohmura et al. 1998).

The BSRN has a network of 56 stations with several candidate stations. 35 stations were delivering data at the time that the data was collected for the present study and 31 of those were within the field of view of the satellites used (see Figure 3.2 and Table 3.2). The network was chosen as the source of ground truth data due despite its low number of stations due to their global distribution and the fact that the data they collect contains both surface solar global and direct irradiation (World Radiation Monitoring Center – Baseline Surface Radiation Network 2012b). For more information about the BSRN stations and what variables they measure, see chapter 2.1.2.

Additional quantitative SIS validation data was obtained from the ERA-Interim archive (Dee et al. 2011) and the CLARA surface radiation product from CM SAF (Trentmann, Müller, et al. 2012a). Unfortunately, these data sources did not provide SID and CAL.

Qualiative validation was performed using the MODIS cloud fraction product (National

Aeronautics and Space Administration 2012). It utilizes several spectral bands that are observed using the MODIS instrument, as well as a comprehensive suite of ancillary data on land cover, topography, solar geometry, and surface temperature to assess the degree of cloudiness in an observed pixel. The final product is composed of 1 km pixels, whose values are the percentage of 250 m pixels contained in each 1 km window that are identified with a high degree of confidence as being cloudy (Ackerman et al. 2010). Although the MODIS instrument is available onboard both the Terra and the Aqua polar orbiting satellites, only data collected on the Aqua satellite was utilized in this paper. This is due to the fact that Aqua's orbit is on a sun-synchronous ascending node which observes at 13:30 local solar time, whereas Terra observes on a 10:30 descending node (Maccherone 2012). The noontime observations were assumed to contain higher contrast, making it easier to qualitatively compare the cloud fraction product with the CAL, SID and SIS products produced in the course of this thesis. For each satellite, an observation near local noon was used from the 1st, 15th and 30th day of the month tested.

Table 3.2: Relevant BSRN station names, positions and elevations. Based on: (World Radiation Monitoring Center – Baseline Surface Radiation Network 2012a).

Station Name	Position (°N, °E)	Elevation (a.s.l.)
Alice Springs	-23.8°, 133.9°	547 m
Bermuda	32.3°, -64.7°	8 m
Billings	36.6°, -97.5°	317 m
Bondville	40.1°, -88.37°	1689 m
Boulder	40.1°, -105.2°	1689 m
Boulder	40.1°, -105.0°	1577 m
Camborne	50.2°, -5.3°	88 m
Carpentras	44.1°, 5.1°	100 m
Chesapeake Light	36.9°, -75.7°	37 m
De Aar	-30.7°, 24.0°	1287 m
Darwin	-12.4°, 130.9°	30
Desert Rock	36.6°, -116.0°	1007 m
S. Great Plains	36.6°, -97.5°	318 m
Fort Peck	48.3°, -105.1°	634 m
Goodwin Creek	34.3°, -89.9°	98 m
Ilorin	8.5°, 4.6°	350 m
Kwajalein	8.7°, 167.7°	10 m
Lauder	-45.0°, 169.7°	350 m
Lerwick	60.1°, -1.2°	84 m
Lindenberg	52.2°, 14.1°	125 m
Momote	-2.1°, 147.4°	6 m
Nauru Island	-0.5°, 166.9°	7 m
Palaiseau, SIRTA Observatory	48.7°, 2.2°	156 m
Payerne	46.8°, 6.9°	491 m
Rock Springs	40.7°, -77.9°	376 m
Regina	50.2°, -104.7°	578 m
Sede Boger	30.9°, 34.8°	500 m
Sioux Falls	43.7°, -96.6°	473 m
Tamanrasset	22.8°, 5.5°	1385 m
Tateno	36.1°, 140.1°	25 m
Toravere	58.3°, 26.5°	70 m

4. Methods

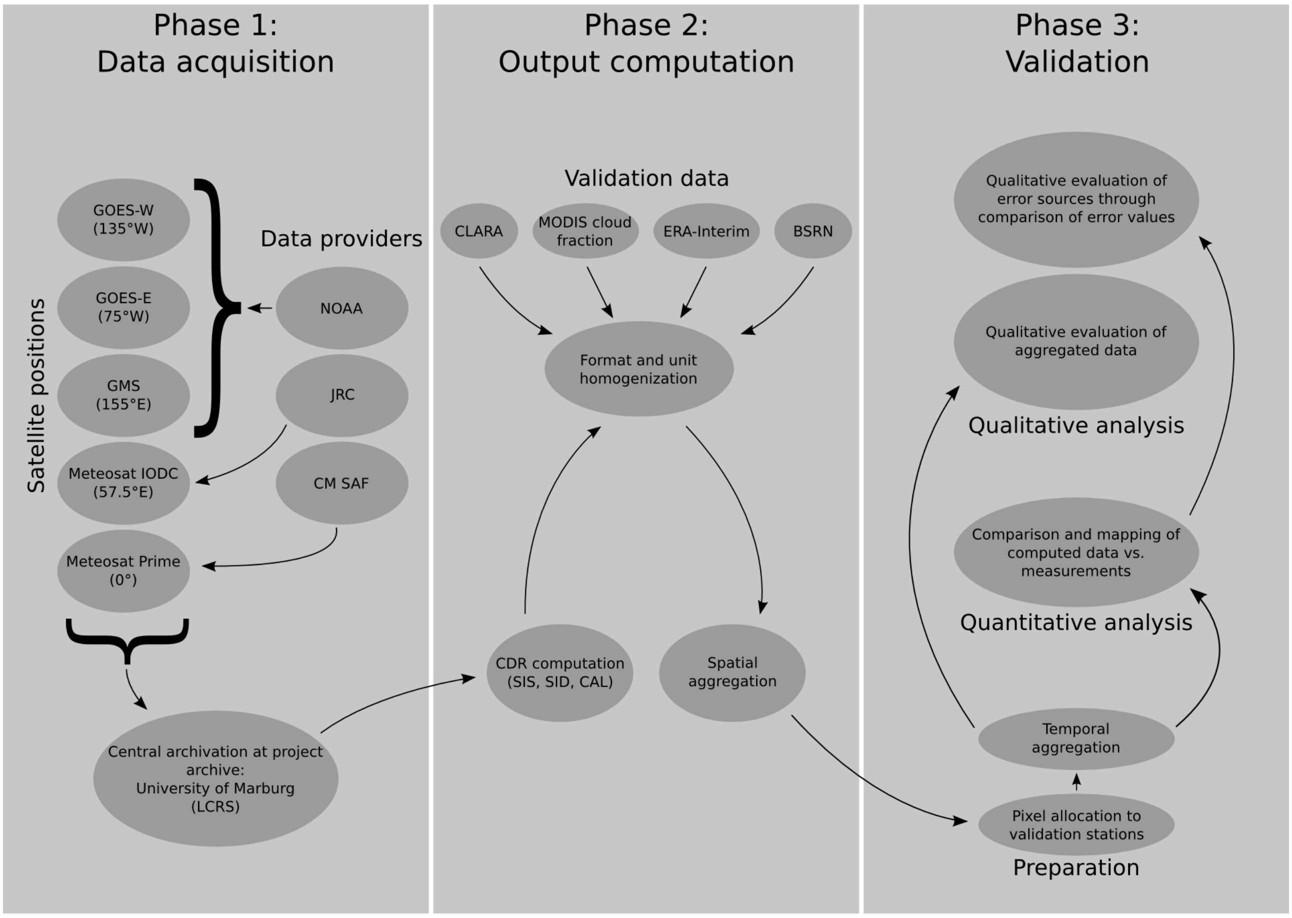

Figure 4.1: Workflow diagram of the three phases of the empirical investigation.

The empirical portion of this thesis was performed in three phases: (i) data acquisition, (ii) output computation and (iii) validation (see figure 4.1). In phase (i), data concerning each satellite was collected and archived from the data providers. In phase (ii), the CDRs were computed for all GOES satellites. After that, the produced data, as well as the validation data, was reformatted into a single format and the units converted, if needed, to W/m². Finally, a map combining each globally available time step was created by merging the relevant scans of each satellite processed. Phase (iii) began with the temporal aggregation of all computed and measured data to create a temporally homogeneous basis of comparison. Afterwards, the computed data was compared with the validation data at various temporal aggregation levels. Finally, the entire data was evaluated as a whole. Additionally, error sources were sought by examining the scores of individual station sites and satellites.

4.1. Data acquisition

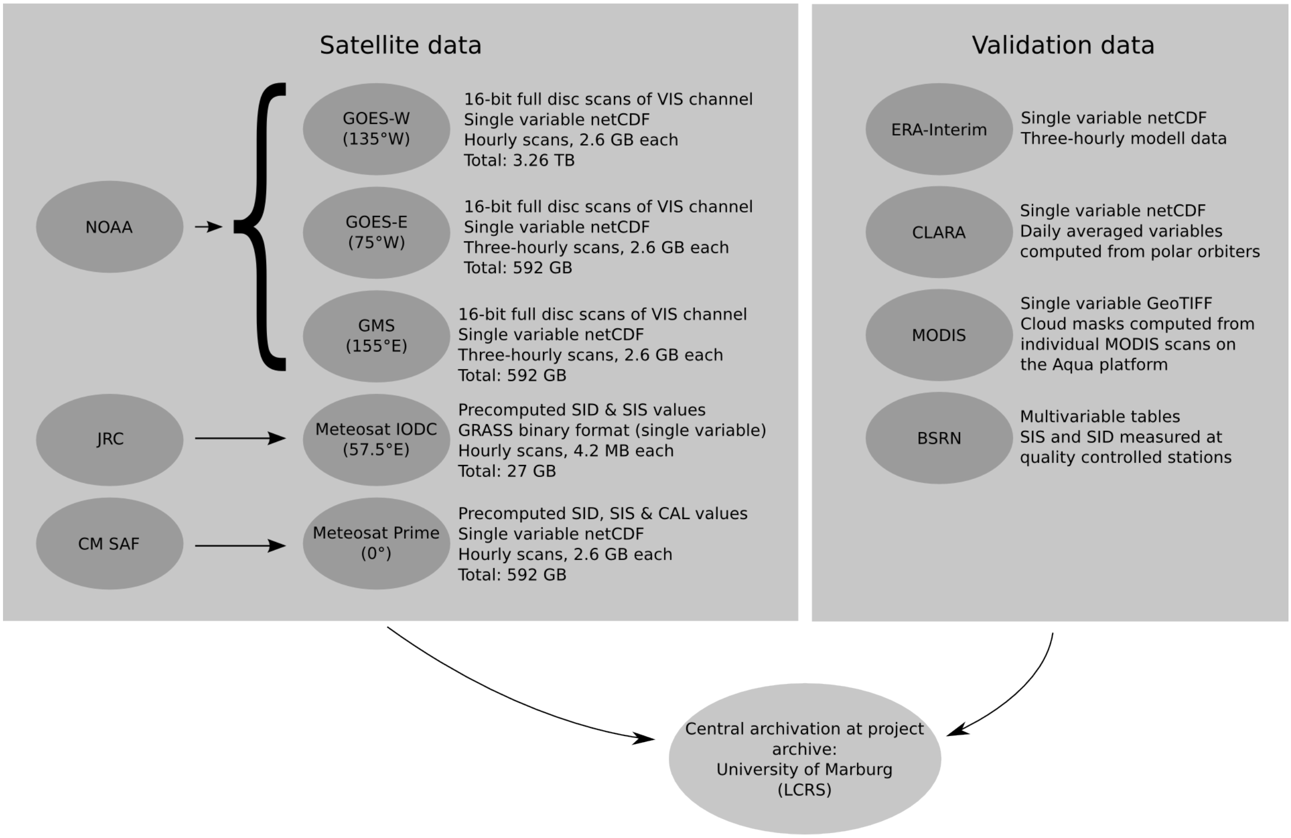

Figure 4.2: Workflow diagram of phase i: data acquisition.

As a first step, all data had to be acquired and centrally archived (see Figure 4.2). Due to the large amount of data, this was accomplished using scripts.

Data from the three GOES satellites that were used was ordered and downloaded from NOAA's Comprehensive Large Array-data Stewardship System (CLASS) (NOAA US Department of Commerce 2012b). The data was available in netCDF format with 16 bits per pixel, so that each full disc scan file required 2.6 GB disk space. Because only 100 scans could be ordered simultaneously, several orders were placed at once. GOES-9++ performed full disc scans each hour and sometimes even more frequently, requiring 836 downloads totaling 2.1 TB disc space. GOES-10 scanned every three hours and, when needed, every half hour, requiring 236 downloads for a total of 592 GB. GOES-12 also scanned every three hours, requiring 243 downloads for a total of 592 GB. In total, the GOES data amounted to 3.26 TB.

Because CLASS products are only available for 120 hours after ordering, several orders had to be placed. Downloads were conducted over more than four weeks using a download accelerator, Aria2, which opens multiple connections to a host and splits files into chunks that are then downloaded in parallel (Tsujikawa 2012). This made it possible to download the data within the project time frame.

The necessary CDRs for the Meteosat-Prime coverage area were already available directly from CM SAF. They were ordered and downloaded from the CM SAF web user interface as netCDF files and required a total of 27 GB disk space (EUMETSAT Satellite Application Facility on Climate Monitoring 2012).

The PVGIS project at the JRC had also used the MAGICSOL method to create data sets of SIS and SID. At the author's request, the preliminary, unpublished results were made available as a GRASS GIS database with a disk size of 6 GB (Huld 2012).

Validation data from BSRN was made available directly through the project's FTP server (World Radiation Monitoring Center – Baseline Surface Radiation Network 2012c). The files were in the complex station-to-archive files and were converted into comma separated tables using the BSRN toolbox for analysis (Sieger 2012). MODIS cloud masks were ordered from the LAADS platform (National Aeronautics and Space Administration 2012). Before they were downloaded, they were georeferenced and converted into the GeoTIFF format on the server. ERA-Interim downwelling surface irradiation data was downloaded from the ECMWF server (European Centre for Medium-Range Weather Forecasts 2012). SIS data computed from AVHRR was downloaded from the CM SAF Web User Interface (EUMETSAT Satellite Application Facility on Climate Monitoring 2012).

4.2. Output computation

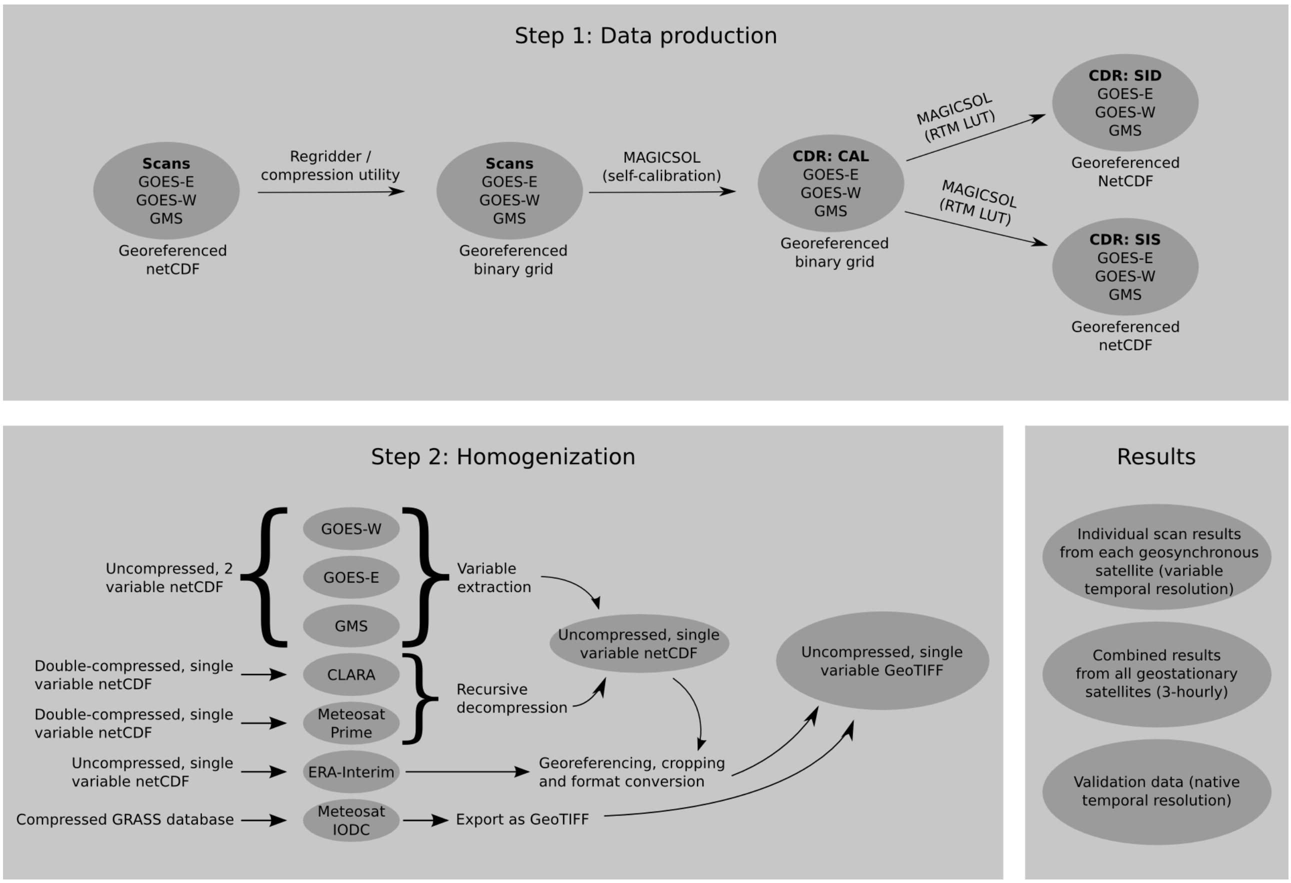

Figure 4.3: Workflow diagram of phase ii: output computation.

Several steps were necessary in order to convert the raw data from the satellites into CDR. First, the data was preprocessed and outputs were computed. Then the produced data, as well as the validation data, were converted into a single format to allow intercomparison. Finally, several additional, aggregated outputs were produced in order be able to qualitatively evaluate the agreement between satellites, as well as their ability to detect global-scale phenomena (see Figure 4.3).

In the first step, the scan data received from NOAA for the GOES-E, GOES-W and GMS positions was preprocessed using a regridding and compression utility (Müller 2012). This was done in order to convert the netCDF files provided NOAA into a binary format which could be directly used by the MAGICSOL software. The result was a collection of scans from each of the aforementioned satellites, converted into the binary XPIF format, reduced to 8-bit precision and warped onto a regular lat-lon grid with a horizontal resolution of 0.02° (approximately 2 km at the equator).

After the data was regridded, it was used to calculate the cloud albedo for each time step. This was done using the MAGICSOL software suite, which is based on the Heliosat algorithm (Cano et al. 1986). The following section briefly explains the MAGICSOL method; the complete details can be found in (R. Mueller, Trentmann, Träger-Chatterjee, et al. 2011).

First, the satellite counts observed at each pixel were normalized to correct for differences in illumination effects resulting from the satellite's viewing angle and the solar geometry relative to the earth at the observed point. Then the clear-sky reflectance (ρ_{cs}) for each pixel and time slot was computed by comparing each pixel observation over the course of seven days. The minimum reflectance for those seven days was assumed to correspond to a clear-sky observation of the ground at the pixel in question. This allowed for changes in ground-cover that affect the pixel's albedo to be detected and compensated for in the course of the month.

The maximal reflectance for the current state of the satellite's radiometer at the time of the observation was computed by observing a target region with a high number of compact clouds. As each satellite had a large amount of ocean in its field of view, providing a well-suited window for observing compact cloud decks, the “Roaring Forties” between 40°S and 50°S was used as a target area. For each satellite, the 95th percentile normalized counts of the near-noontime slot in this area was used to find the highest observable reflectance (ρ_{max}) for the satellite in question at that point in time. Using the 95th percentile rather than the absolute maximum created more stable maximum values, as especially high observations resulting from sensor saturation were excluded. Subsequently, the effective cloud albedo (*CAL*) was computed for each observation of each pixel using the following formula:

$$CAL=\frac{\rho-\rho_{cs}}{\rho_{max}-\rho_{cs}} \tag{1}$$

Additionally, a snow test was applied to distinguish between albedo changes caused by cloud and snowfall, as outlined in (Rebekka Posselt et al. 2011). This test assumes that consistently high pixel albedo points to snow cover, whereas variably high albedos can more readily be attributed to clouds. If snow is detected, ρ_{cs} is artificially raised for the pixel in question to compensate for the snow's high albedo.

Both the surface incoming shortwave radiation (SIS) and surface incoming direct radiation (SID) were then computed using the climatologies described in chapter 3.2 and the cloud albedo as inputs for an eigenvector-based look-up-table (LUT) approach (R. W. Mueller et al. 2009). This method interpolates between precomputed results of radiative transfer model runs, which were calculated using the libRadtran RTM (Mayer and Kylling 2005).

4.3. Validation

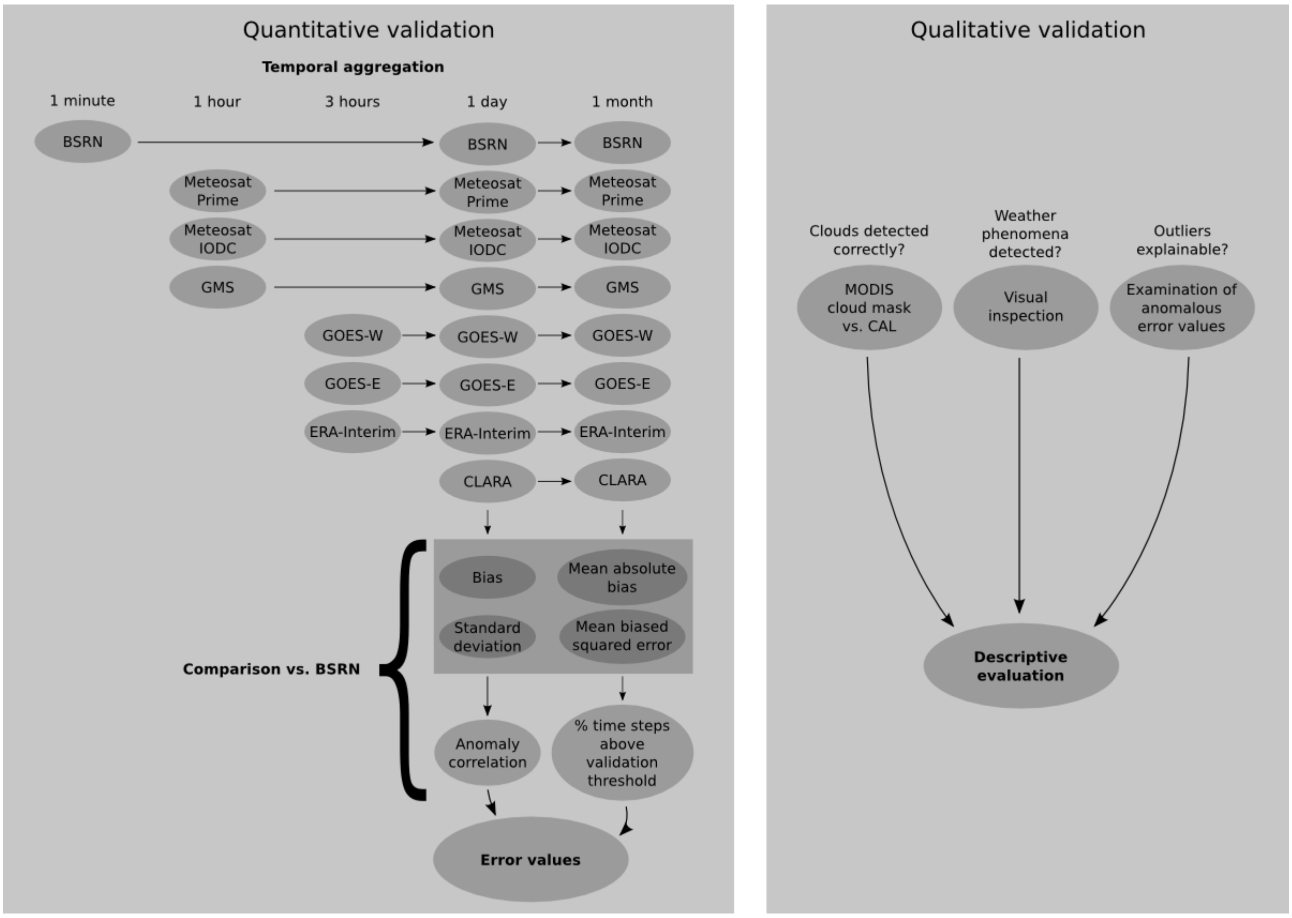

Figure 4.4: Workflow diagram of phase iii: validation.

In the third phase, the produced data was evaluated both quantitatively and qualitatively. For an overview of both validation processes, see Figure 4.4.

The quantitative validation was performed by comparing the data produced with the accuracy of the ERA-Interim and CLARA data under the assumption that the BSRN station data was correct. Because no direct measurements for effective cloud albedo (CAL) were available, only surface incoming shortwave radiation (SIS) and surface incoming direct radiation (SID) were validated numerically.

To provide a comparable basis of comparison for all data sets, the data were first temporally aggregated to a common resolution. The BSRN data was available as minute-by-minute measurements, whereas the Meteosat-Prime, Meteosat-IODC and GMS scans were available hourly. GOES-W and GOES-E, as well as the ERA-Interim validation data, were only available in three-hourly resolution, and the CLARA data was available only on a daily basis. Thus the SIS and SID values were first aggregated to daily sums of Wh/m². Additionally, they were aggregated to monthly sums in order to compare the accuracy of each data set of the course of the entire month. Because the ERA-Interim and CLARA data contained only SIS data, the SID data produced using MAGICSOL was compared only with the BSRN measurements.

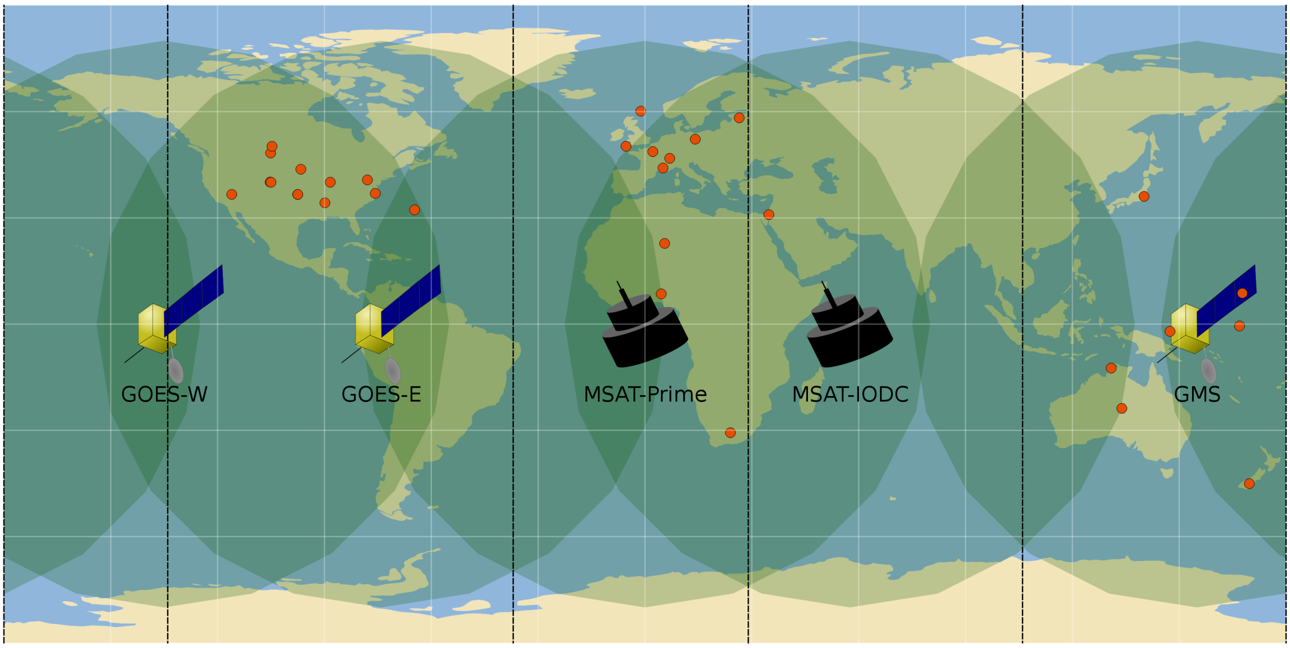

Figure 4.5: Satellite viewing areas. Individual satellites are shown on the map. The ellipses beneath them denote the satellite's viewing geometry. Black dotted lines denote borders between satellite domains used in this study, points are BSRN stations used for validation. Based in part on: (NOAA US Department of Commerce 2012a; EUMETSAT 2012).

After aggregating the data, the values in the data set was extracted at the position of the validation stations for each time step. For an overview of the stations used and the satellites they were assigned to, see Figure 4.5.

each data set was evaluated based on the following error values, according to (Wilks 2005) and (R. Posselt, Müller, Trentmann, et al. 2011). In each equation, *y* stands for a predicted value, *o* for the corresponding value measured at the BSRN station, *k* for a given sample at a point in time and *n* the total number of samples.

$$Bias=\frac{1}{n}\sum_{k=1}^{n}(y_k-o_k) \qquad (2)$$

The bias, or mean error, shows the mean difference between two data sets. A negative bias indicates that the predicted values are generally lower than the observed data, whereas a positive bias reflects an overestimation compared with the observed data. One weakness of this value is that positive and negative differences between the observed and predicted data effectively cancel each other out.

$$MAD = \frac{1}{n} \sum_{k=1}^{n} |y_k - o_k| \tag{3}$$

The mean absolute difference (MAD) is computed similarly to the bias, but the magnitude of the difference between the two data sets, rather than its direction, is evaluated. MAD is a more general value for how much one data set deviates from another.

$$SD = \sqrt{\frac{1}{n-1} \sum_{k=1}^{n} ((y_k - o_k) - (\bar{y}_k - \bar{o}_k))^2} \tag{4}$$

The standard deviation (SD) measures the variability of the differences between two data sets. It is a measure for the variability of the deltas between the generated and observed data.

$$AC = \frac{\sum_{k=1}^{n} (y_k - \bar{y})(o_k - \bar{o})}{\sqrt{\sum_{k=1}^{n} (y_k - \bar{y})^2} \sqrt{\sum_{k=1}^{n} (o_k - \bar{o})^2}} \tag{5}$$

The anomaly correlation (AC) shows how much a given sample deviates from the monthly mean of all samples in that data set. It shows to what extent deviations from each data set's mean are reflected in the other data set, making it possible to see whether similar phenomena are observed in two data sets, independent of any systematic bias contained in either one. Because only one month of data was computed, the AC was only computed for the daily data as compared to the monthly mean.

$$RMSE = \sqrt{\frac{1}{n} \sum_{k=1}^{n} (y_k - o_k)^2} \tag{6}$$

The root mean squared error (RMSE) is a measure for the magnitude of differences between two data sets, similar to the MAD. However, because the values measured are squared, RMSE is more sensitive to outliers.

$$frac = \frac{t}{n} \tag{7}$$

The fraction of time steps above the validation threshold is a measure of the proportion of the generated data whose accuracy is lower than the target accuracy. In this case, *t* denotes the number of samples who deviate more from the BSRN samples than allowed. The thresholds for each variable and time step can be found in Table 1.1.

The qualitative validation was performed by examining various aspects of the data manually. First, MODIS cloud masks were compared with the cloud albedo values generated by the MAGICSOL software. It was assumed that if the cloud mask would correspond with high cloud albedo values generated by MAGICSOL.

Additionally, the scans from each individual satellite were merged into a single, global image. Because the highest temporal resolution was three-hourly, one image was made for every three hours. Where possible, scans beginning simultaneously were combined. When this was not possible, the closest scan begin was used. The largest difference between scan start times for combined imagery was 25 minutes, ensuring the most simultaneous unified geosynchronous scan possible (see Table 4.1). Because CAL was not available for Meteosat-IODC coverage, global images were only created for SIS and SID.

Table 4.1: Scan times that were used to create combined, global imagery.

Satellite / Time slot (UTC +0)	**0000**	**0300**	**0600**	**0900**	**1200**	**1500**	**1800**	**2100**
GOES-W	0000	0300	0600	0900	1200	1500	1800	2100
GOES-E	2345	0245	0545	0845	1145	1445	1745	2045
Meteosat-Prime	0000	0300	0600	0900	1200	1500	1800	2100
Meteosat-IODC	0000	0300	0600	0900	1200	1500	1800	2100
GMS	0025	0325	0625	0925	1225	1525	1825	2125

These pictures were examined in order to determine whether phenomena could be observed across several satellites and to qualitatively evaluate the plausibility of the generated values. Of the 240 3-hourly time steps in the study period, 16 scans were missing. These time steps were not used to make global images.

Finally, the error values produced during the quantitative validation were examined qualitatively in order to examine possible causes for especially good or bad scores.

5. Results and discussion

In the following, the results are introduced and discussed in detail.

5.1. Regridding

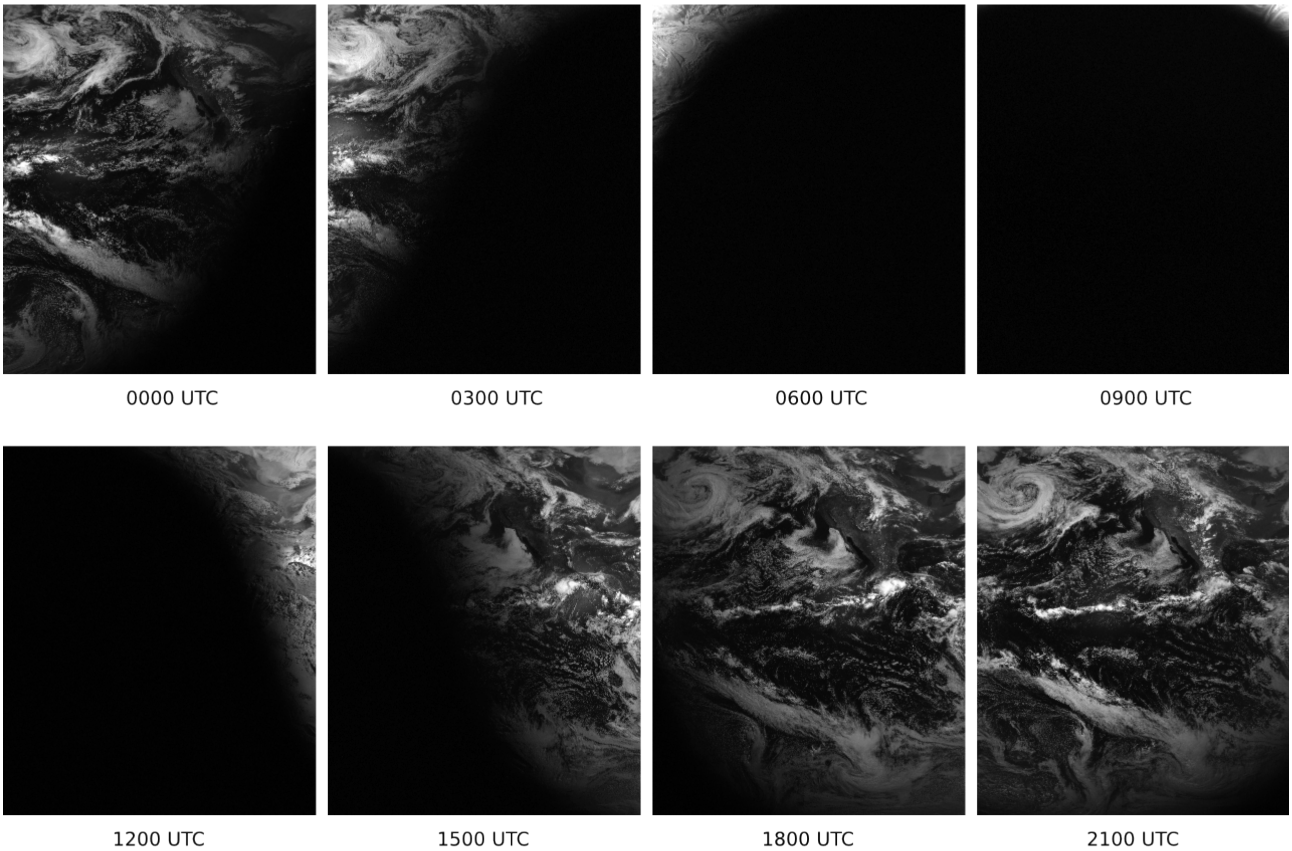

Figure 5.1: Typical day for GOES-W (152).

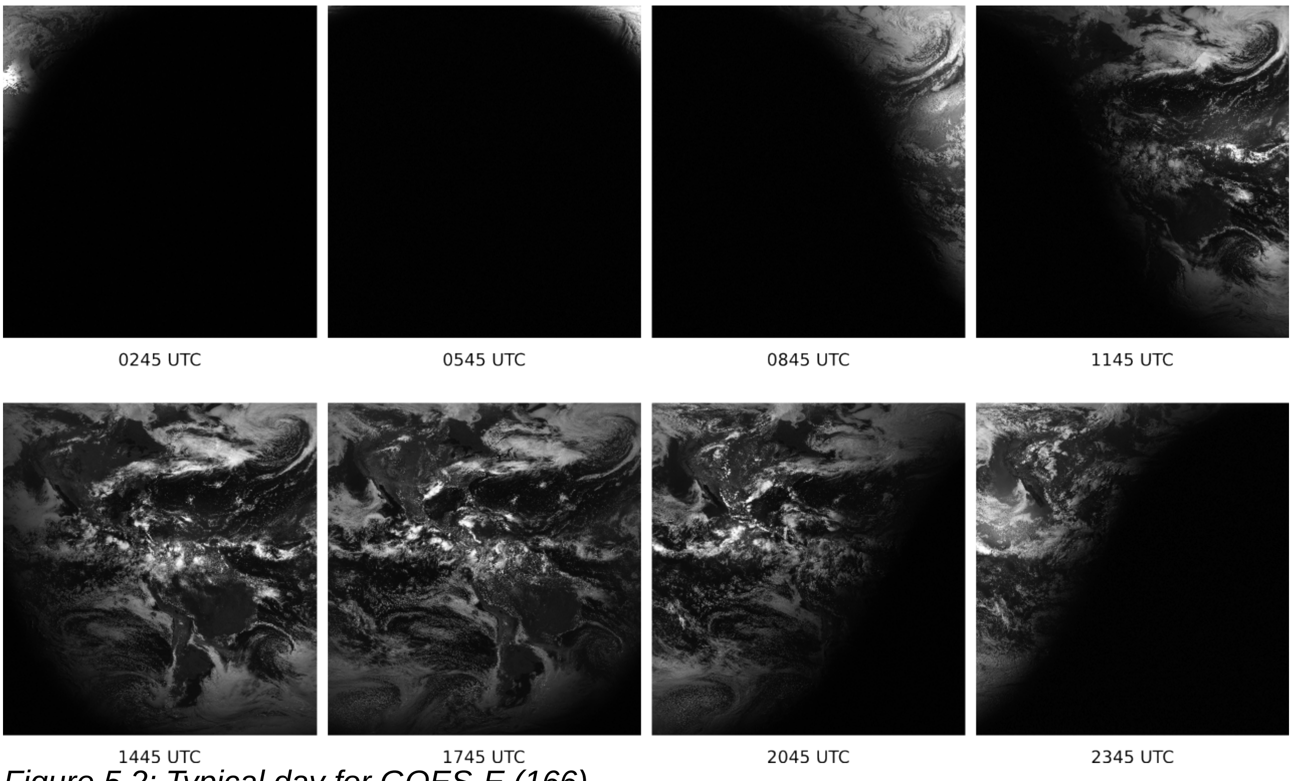

Figure 5.2: Typical day for GOES-E (166).

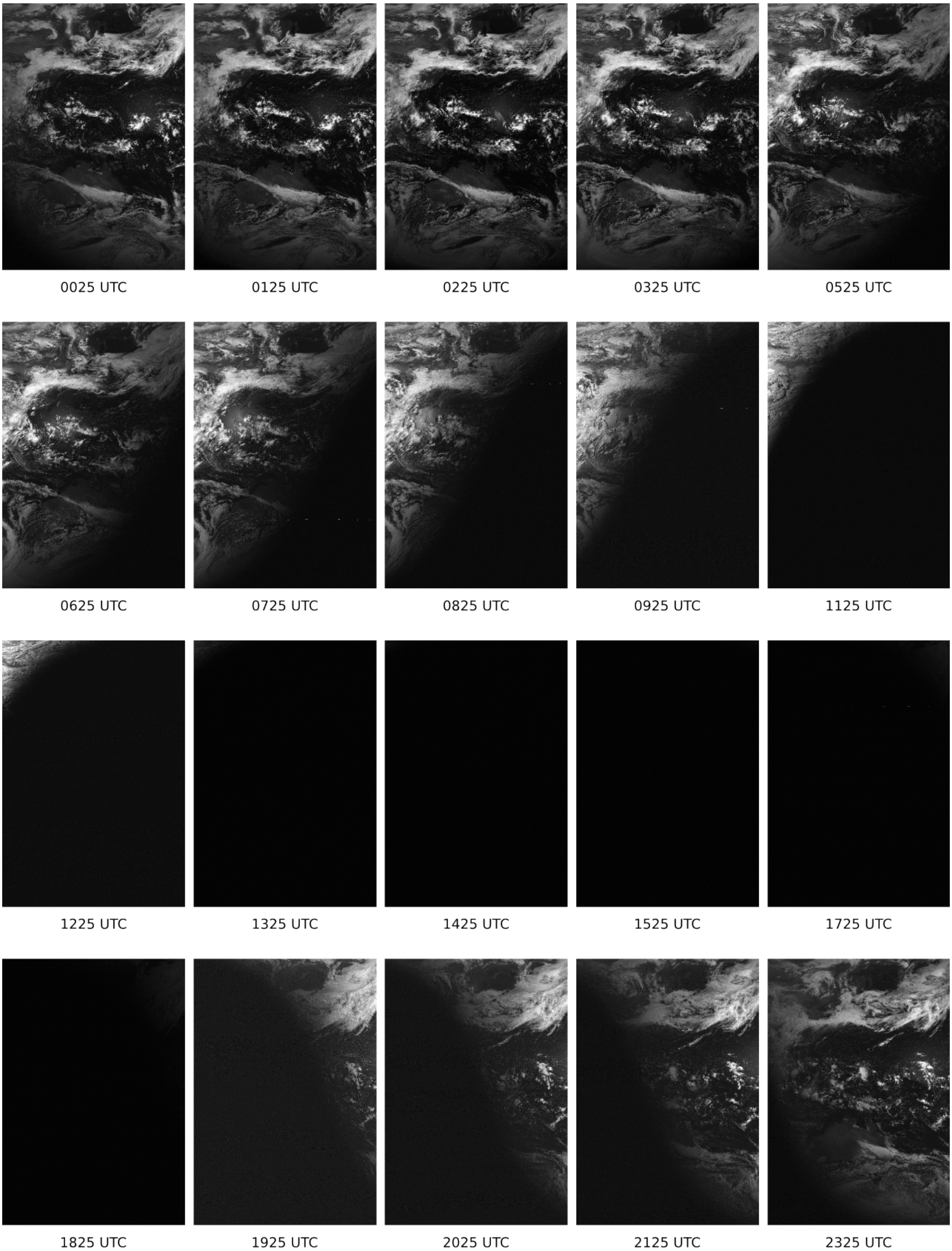

Figure 5.3: Typical day for GMS (181).

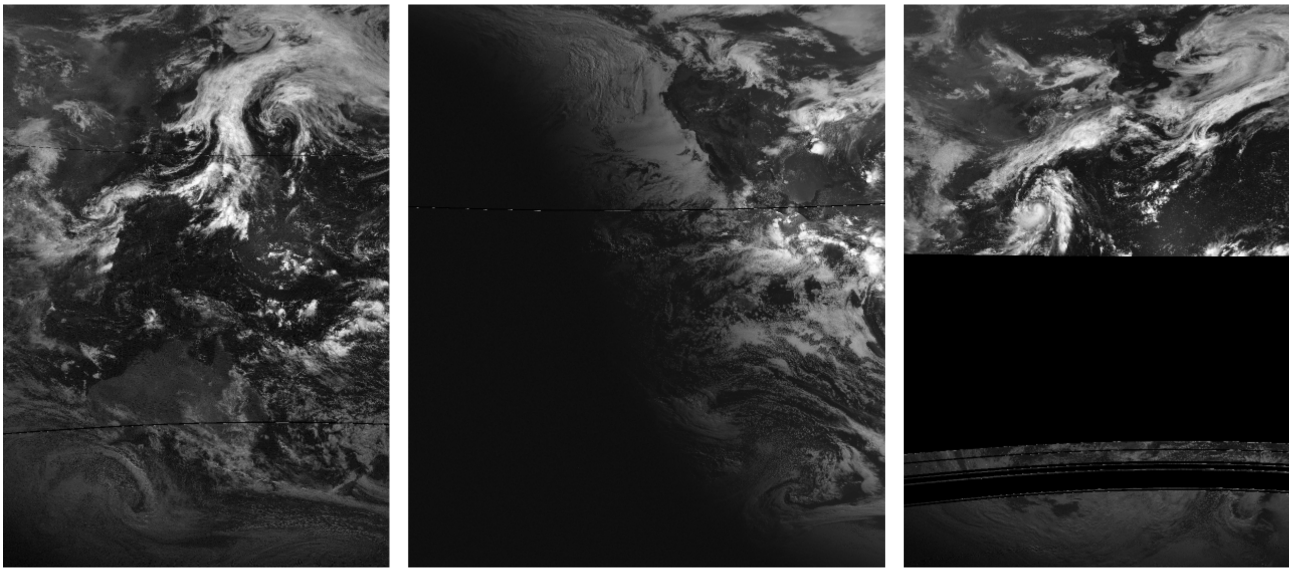

GOES-9++, day 152, 0125 UTC
GOES-10, day 162, 1500 UTC
GOES-9++, day 167, 0125 UTC

Figure 5.4: Examples of scan errors.

Maps of the regridded observations. Typical days. Scan errors.

Table 5.1: Satellite scan errors that were found during visual evaluation of the scans used for the study. All scan errors that could be visually identified were noted. Most errors were minor, being restricted to a single line and were ignored. Major scan errors led to a scan not being included in the following steps.

Satellite	Minor errors	Major errors	Errors / Total scans	Notes
GOES-9++ (GMS)	65	2	67 / 596	
GOES-10 (GOES-W)	1		1 / 232	
GOES-12 (GOES-E)	0	10	10 / 240	Scans with errors were missing

5.2. Cloud albedo

Cloud albedo maps. Also comparison maps.

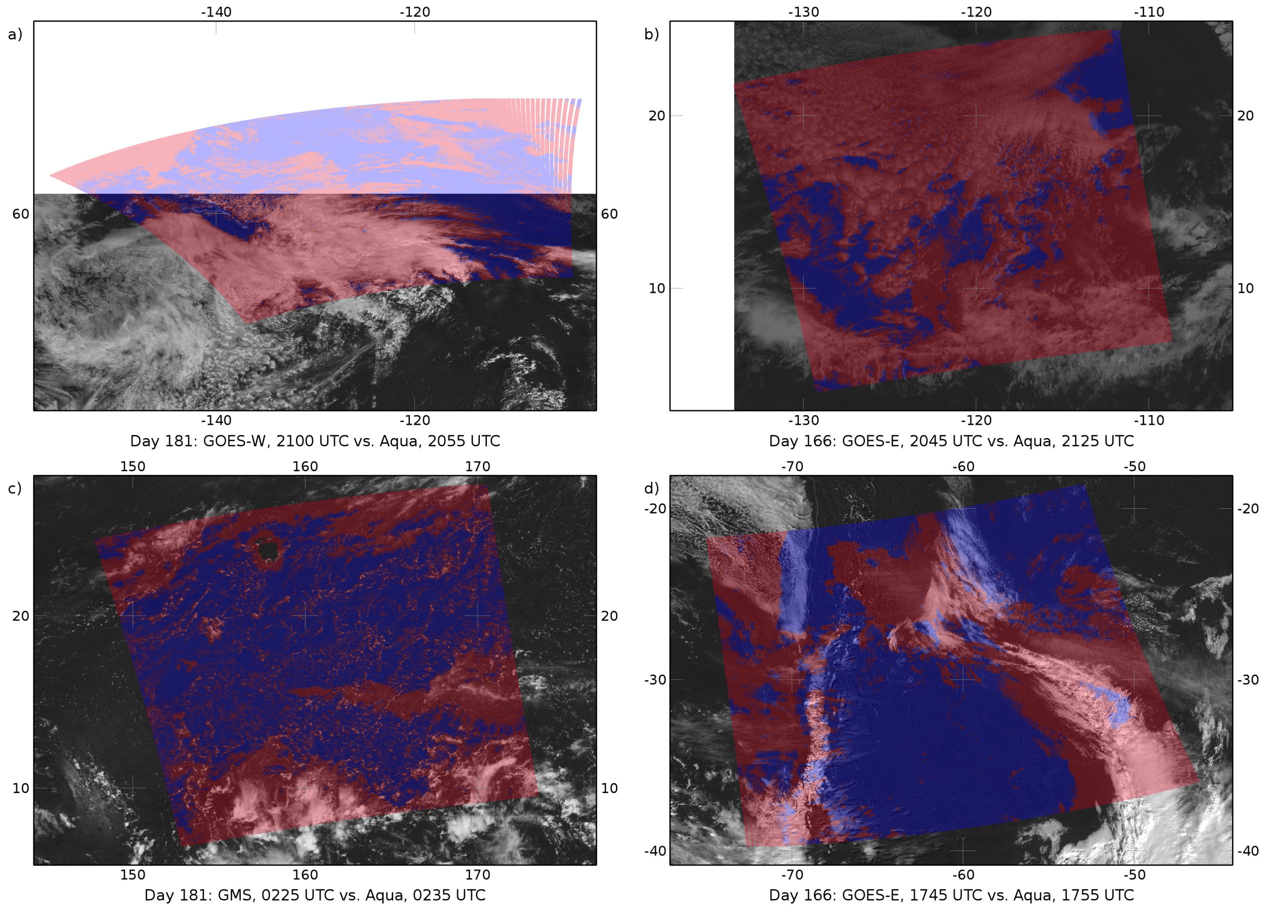

Figure 5.5: Examples of generated CAL values compared to MODIS cloud fraction maps. The generated CAL values are in gray tones, with brighter pixels denoting higher effective cloud albedo. The MODIS cloud fraction is classified on a blue-to-red scale, with blue denoting low cloud cover and red high cloud cover. Based partly on (National Aeronautics and Space Administration 2012).

a-c are good, d looks kinda bad but it's probably because the clouds were moving fast. 1755 was the Aqua scan and the GOES scan started at 1745, so it probably took the picture a little later.

5.3. SID

5.4. SIS

Remember: Some scans were missing, mention it.

Show:

- Typical days of SID/SIS/CAL for GOES, each satellite and then global. Style them nicely (b/w)
- Scan errors from each satellite (which pictures had to be thrown out?)

- Combined product of all satellites – typical day. Possible to see weather phenomena?
- Monthly average
- Difference pictures GOES-E/Meteosat Prime? Meteosat IODC/GMS? GOES-W/GOES-E? Statistics – descriptive statistics (STD, AVG/MAX/MIN of each)
- Comparison CAL w/ MODIS cloud product – if there's not much time with SID
- Tables – error statistics between ERA, CLARA, data produced

6. Discussion

- Good idea for next time: Produce eastern data with GOES-W, because it really sucks not to have validated it.
- Validation results – satellite specific? Intercomparison in overlapping satellite FOVs? Do the different sensors make a difference?
- Pixel size → ERA: 0.75°. CLARA: 0.25. Geo: 0.1 possible.
- Comparison to similar data sets
- Feasibility in expanding temporal coverage
- Feasibility in expanding spatial coverage
- *For validation remember to take a look at the other data sets – ERA Interim & CLARA – use Posselt's stuff to compare accuracy per satellite and then for the entire data set*
- Can I see ITCZ and stuff?
- Compare with MODIS cloud product
  - Data availability
- Possibility of using AVHRR as supplement

7. Conclusions

Short and simple, how well the method worked.

- Practical uses

- Possibilites of improvement: Cross-calibration, updated climatologies
- Combination geostationary / AVHRR

Acknowledgments

Thanks to Jörg Bendix, Richard Müller and Thomas Huld for their support in technical and theoretical aspects of the work. Thanks to EUMETSAT and NOAA for providing data. Thanks to the open source community, especially GRASS GIS, Python, R, QGIS, OpenSUSE and Zotero. Thanks to the ISIS team for carrying the torch while I was away. Thanks to the many unnamed people that helped with their ideas, proofreading, and psychological support. Also to netCDF.

Bibliography

Ackerman, Steve, Richard Frey, Kathleen Strabala, Yinghui Liu, Liam Gumley, Bryan Baum, and Paul Menzel. 2010. "Discriminating Clear-sky from Cloud with MODIS." *Algorithm Theoretical Basis Document: Cooperative Institute for Meteorological Satellite Studies, University of Wisconsin - Madison* 6.1 (October).

Berrisford, Paul, D. Dee, K. Fielding, M. Fuentes, P. Kallberg, S. Kobayashi, and S. Uppala. 2009. "The ERA-Interim Archive." *ERA Report Series*. http://www.ecmwf.int/publications/library/do/references/list/782009.

Bishop, James K. B., William B. Rossow, and Ellsworth G. Dutton. 1997. "Surface solar irradiance from the International Satellite Cloud Climatology Project 1983–1991." *Journal of Geophysical Research* 102 (D6) (March 27): 6883–6910. doi:10.1029/96JD03865.

Bureau of Meteorology, Commonwealth of Australia. 2012. "Solar and Terrestrial Radiation." http://www.bom.gov.au/climate/austmaps/solar-radiation-glossary.shtml#pyranometers.

Cano, D., J.M. Monget, M. Albuisson, H. Guillard, N. Regas, and L. Wald. 1986. "A Method for the Determination of the Global Solar Radiation from Meteorological Satellite Data." *Solar Energy* 37 (1): 31–39. doi:10.1016/0038-092X(86)90104-0.

Chou, Ming-Dah, and Max J. Suarez. 1999. "A Solar Radiation Parametrization for Atmospheric Studies." *Technical Report Series on Global Modeling and Data Assimilation* 15 (June).

Dee, D. P., S. M. Uppala, A. J. Simmons, P. Berrisford, P. Poli, S. Kobayashi, U. Andrae, et al. 2011. "The ERA-Interim Reanalysis: Configuration and Performance of the Data Assimilation System." *Quarterly Journal of the Royal Meteorological Society* 137 (656): 553–597. doi:10.1002/qj.828.

Deneke, H.M., A.J. Feijt, and R.A. Roebeling. 2008. "Estimating Surface Solar Irradiance from METEOSAT SEVIRI-derived Cloud Properties." *Remote Sensing of Environment* 112 (6) (June): 3131–3141. doi:10.1016/j.rse.2008.03.012.

Department of Primary Industries, State Government of Victoria. 2011. "Renewable Energy Report Part 2." *Department of Primary Industries, Victoria, Australia*. http://www.dpi.vic.gov.au/energy/sustainable-energy/renewable/part-2.

Diak, George R., William L. Bland, and John Mecikaski. 1996. "A Note on First Estimates

of Surface Insolation from GOES-8 Visible Satellite Data.” *Agricultural and Forest Meteorology* 82 (1–4) (December): 219–226. doi:10.1016/0168-1923(96)02331-3.
Diak, George R., Catherine Gautier, and Serge Masse. 1982. “An Operational System for Mapping Insolation from Goes Satellite Data.” *Solar Energy* 28 (5): 371–376. doi:10.1016/0038-092X(82)90254-7.
EUMETSAT. 2012. “EUMETSAT - Satellites - Mission Overview.” http://www.eumetsat.int/Home/Main/Satellites/MeteosatFirstGeneration/MissionOverview/index.htm?l=en.
EUMETSAT Satellite Application Facility on Climate Monitoring. 2012. “CM SAF Web User Interface - Home.” http://wui.cmsaf.eu/safira/action/viewHome;jsessionid=369137C316F1D8735365CCB6EC9F4956.ku_1.
European Centre for Medium-Range Weather Forecasts. 2012. “ERA Interim, Daily Fields, Full Resolution.” http://data-portal.ecmwf.int/data/d/interim_full_daily/.
European Union. 2012. “JRC’s Institute for Energy and Transport - PVGIS - European Commission.” http://re.jrc.ec.europa.eu/pvgis/.
Flowers, E. 1978. “The NOAA/DOE Solar Radiation Facility and Measurement Network.” In *Seminar on Testing Solar Energy Materials and Systems*, -1:112–116. http://adsabs.harvard.edu/abs/1978stse.proc..112F.
GeoModel Solar s.r.o. 2012a. “SolarGIS: Price List.” *SolarGIS*. http://solargis.info/doc/5.
———. 2012b. “SolarGIS Database: Satellite-to-irradiance Model.” *SolarGIS*. http://solargis.info/doc/109.
Gesell, G. 1989. “An Algorithm for Snow and Ice Detection Using AVHRR Data An Extension to the APOLLO Software Package.” *International Journal of Remote Sensing* 10 (4-5): 897–905. doi:10.1080/01431168908903929.
Global Climate Observing System. 2012. “GCOS Essential Climate Variables.” *World Meteorological Organization* (June 4). 2011. http://www.wmo.int/pages/prog/gcos/index.php?name=EssentialClimateVariables.
Gupta, Shashi K., David P. Kratz, Paul W. Stackhouse, Anne C. Wilber, Taiping Zhang, and Victor E. Sothcott. 2010. “Improvement of Surface Longwave Flux Algorithms Used in CERES Processing.” *Journal of Applied Meteorology and Climatology* 49 (7) (July): 1579–1589. doi:10.1175/2010JAMC2463.1.
Hammer, Annette. 2001. “Anwendungsspezifische Solarstrahlungsinformationen aus Meteosat-Daten”. Oldenburg: Carl-von-Ossietzky-Universtität Oldenburg. http://oops.uni-oldenburg.de/frontdoor.php?source_opus=347.
Hegner, H., G. Müller, V. Nespor, A. Ohmura, R. Steigrad, and H. Gilgen. 1998. “World Climate Research Program WCRP (WMO/ICSU/IOC) Baseline Surface Radiation Network (BSRN) Update of the Technical Plan for BSRN Data Management.” *Institute of Geography ETH Zurich, Switzerland, World Radiation Monitoring Center (WRMC) Technical Report* 2, Version 1.0 (October 9). http://www.springerlink.com/index/Q88178XV5N6MH452.pdf.
Huld, Thomas. 2012. “Re: Protocol & Info from Meeting on 28.8.2012.”
Huld, Thomas, and Ewan Dunlop. 2012a. “PVGIS - Frequently Asked Questions About PVGIS and Interactive Maps.” *JRC’s Institute for Energy and Transport - PVGIS - European Commission*. http://re.jrc.ec.europa.eu/pvgis/info/faq.htm.
———. 2012b. “PVGIS - Solar Radiation (Europe) in PVGIS.” *JRC’s Institute for Energy and Transport - PVGIS - European Commission*. http://re.jrc.ec.europa.eu/pvgis/solres/solrespvgis.htm#Comparison.
Huld, Thomas, and Ewan D. Dunlop. 2010. “PVGIS New Features.” *JRC’s Institute for Energy and Transport - PVGIS - European Commission*.

http://re.jrc.ec.europa.eu/pvgis/PVGIS_new_features.html.
Huld, Thomas, Ralph Gottschalg, Hans Georg Beyer, and Marko Topič. 2010. “Mapping the Performance of PV Modules, Effects of Module Type and Data Averaging.” *Solar Energy* 84 (2) (February): 324–338. doi:10.1016/j.solener.2009.12.002.
Ineichen, Pierre. 2010. “Satellite Based Short Wave Irradiance Validation over Africa”. University of Geneva.
———. 2011. “Five Satellite Products Deriving Beam and Global Irradiance Validation on Data from 23 Ground Stations”. International Energy Agency.
Ineichen, P., and R. Perez. 1999. “Derivation of Cloud Index from Geostationary Satellites and Application to the Production of Solar Irradiance and Daylight Illuminance Data.” *Theoretical and Applied Climatology* 64 (1): 119–130.
Jacobson, Larry, Alan Seaver, and Jiashen Tang. 2011. “AstroCalc4R: Software to Calculate Solar Zenith Angle; Time at Sunrise, Local Noon and Sunset; and Photosynthetically Available Radiation Based on Date, Time and Location.” *Northeast Fisheries Science Center Reference Document* 11 (14) (August): 10.
Japanese Meteorological Agency. 2012. “MTSAT - JMA’s Satellite Home Page - History at a Glance.” http://www.jma.go.jp/jma/jma-eng/satellite/history.html.
Kalnay, E., M. Kanamitsu, R. Kistler, W. Collins, D. Deaven, L. Gandin, M. Iredell, et al. 1996. “The NCEP/NCAR 40-Year Reanalysis Project.” *Bulletin of the American Meteorological Society* 77 (3) (March): 437–471. doi:10.1175/1520-0477(1996)077<0437:TNYRP>2.0.CO;2.
Kinne, S., M. Schulz, C. Textor, S. Guibert, Y. Balkanski, S. E. Bauer, T. Berntsen, et al. 2006. “An AeroCom Initial Assessment – Optical Properties in Aerosol Component Modules of Global Models.” *Atmos. Chem. Phys.* 6 (7) (May 29): 1815–1834. doi:10.5194/acp-6-1815-2006.
Krämer, M., R. Müller, H. Bovensmann, J. Burrows, J. Brinkmann, E. P. Röth, J. U. Grooß, et al. 2003. “Intercomparison of Stratospheric Chemistry Models Under Polar Vortex Conditions.” *Journal of Atmospheric Chemistry* 45 (1): 51–77.
Kratz, David P., Shashi K. Gupta, Anne C. Wilber, and Victor E. Sothcott. 2010. “Validation of the CERES Edition 2B Surface-Only Flux Algorithms.” *Journal of Applied Meteorology and Climatology* 49 (1) (January): 164–180. doi:10.1175/2009JAMC2246.1.
Kratz, D. P., P. W. Stackhouse, A. C. Wilber, P. K. Sawaengphokhai, and S. K. Gupta. 2012. “Derivation of Surface Fluxes Within One Week of Satellite Measurements Using the FLASHFlux Algorithms.” In Munich, Germany.
Lefèvre, M., L. Wald, and L. Diabaté. 2007. “Using Reduced Data Sets ISCCP-B2 from the Meteosat Satellites to Assess Surface Solar Irradiance.” *Solar Energy* 81 (2) (February): 240–253. doi:10.1016/j.solener.2006.03.008.
Lohmann, S., C. Schillings, B. Mayer, and R. Meyer. 2006. “Long-term Variability of Solar Direct and Global Radiation Derived from ISCCP Data and Comparison with Reanalysis Data.” *Solar Energy* 80 (11) (November): 1390–1401. doi:10.1016/j.solener.2006.03.004.
Maccherone, Brandon. 2012. “About MODIS: Specifications.” *MODIS Website*. http://modis.gsfc.nasa.gov/about/specifications.php.
Madigan, Jay. 2011. “What Is the Earth’s Radiation Budget.” *National Aeronautics and Space Administration*. http://science-edu.larc.nasa.gov/EDDOCS/whatis.html.
Matricardi, M., F. Chevallier, G. Kelly, and J. N. Thepaut. 2004. “An improved general fast radiative transfer model for the assimilation of radiance observations.” *Quarterly Journal of the Royal Meteorological Society* 130 (596) (January): 153–173. doi:10.1256/qj.02.181.

Mayer, B., and A. Kylling. 2005. “Technical Note: The libRadtran Software Package for Radiative Transfer Calculations - Description and Examples of Use.” *Atmospheric Chemistry and Physics Discussions* 5 (2): 1319–1381.

Morris, Christopher. 2012. “GOES POES Program: GOES Timeline.” *National Aeronautics and Space Administration: Goddard Space Flight Center*. http://goespoes.gsfc.nasa.gov/timeline.html.

Mueller, Richard, Tanja Behrendt, Annette Hammer, and Axel Kemper. 2012. “A New Algorithm for the Satellite-Based Retrieval of Solar Surface Irradiance in Spectral Bands.” *Remote Sensing* 4 (3) (March 2): 622–647. doi:10.3390/rs4030622.

Mueller, Richard, Jörg Trentmann, Reto Stöckli, and Rebekka Posselt. 2011. “Meteosat (MVIRI) Solar Surface Irradiance and Effective Cloud Albedo Climate Data Sets.” *EUMETSAT Satellite Application Facility on Climate Monitoring, Algorithm Theoretical Baseline Document* (1.1) (January 25): 1–41.

Mueller, Richard, Jörg Trentmann, Christine Träger-Chatterjee, Rebekka Posselt, and Reto Stökli. 2011. “The Role of the Effective Cloud Albedo for Climate Monitoring and Analysis.” *Remote Sensing* 3 (11) (October 25): 2305–2320. doi:10.3390/rs3112305.

Mueller, R.W., C. Matsoukas, A. Gratzki, H.D. Behr, and R. Hollmann. 2009. “The CM-SAF Operational Scheme for the Satellite Based Retrieval of Solar Surface Irradiance — A LUT Based Eigenvector Hybrid Approach.” *Remote Sensing of Environment* 113 (5) (May): 1012–1024. doi:10.1016/j.rse.2009.01.012.

Müller, Richard. 2012. “Gnu_magic.” *GitHub*. https://github.com/erget/gnu_magic.

National Aeronautics and Space Administration. 2012. “LAADS Web - Level 1 and Atmosphere Archive and Distribution System.” http://ladsweb.nascom.nasa.gov/data/search.html.

NOAA US Department of Commerce. 2003. “Geo Sensor Channels.” *National Oceanic and Atmospheric Administration: TeraScan 3.2*. http://psbcw1.nesdis.noaa.gov/terascan/home_basic/geosats_sensors_tables.html#GMS%20Sensor.

———. 2012a. “National Oceanic and Atmospheric Administration (NOAA) Home Page.” http://www.class.ngdc.noaa.gov/release/data_available/goes/index.htm.

———. 2012b. “NOAA’s Comprehensive Large Array-data Stewardship System.” http://www.class.ngdc.noaa.gov/saa/products/welcome;jsessionid=BD13D2EE274A40FC2878A94949BCF809.

Ohmura, Atsumu, Hans Gilgen, Herman Hegner, Guido Müller, Martin Wild, Ellsworth G. Dutton, Bruce Forgan, et al. 1998. “Baseline Surface Radiation Network (BSRN/WCRP): New Precision Radiometry for Climate Research.” *Bulletin of the American Meteorological Society* 79 (10) (October): 2115–2136. doi:10.1175/1520-0477(1998)079<2115:BSRNBW>2.0.CO;2.

Omni Instruments. 2012. “Solar Radiation Sensors in the UK and Europe.” http://www.omniinstruments.co.uk/products/product/solar.id78.html.

Onogi, Kazutoshi, Junichi Tsutsui, Hiroshi Koide, Masami Sakamoto, Shinya Kobayashi, Hiroaki Hatsushika, Takanori Matsumoto, et al. 2007. “The JRA-25 Reanalysis.” *Journal of the Meteorological Society of Japan. Ser. II* 85 (3): 369–432.

Otkin, J. A., M. C. Anderson, J. R. Mecikalski, and G. R. Diak. 2005. “Validation of GOES-based Insolation Estimates Using Data from the US Climate Reference Network.” *Journal of Hydrometeorology* 6 (4): 460–475.

Page, J. K, M. Albuisson, L. Wald, and others. 2001. “The European Solar Radiation Atlas: a Valuable Digital Tool.” *Solar Energy* 71 (1): 81–83.

Pinker, R. T., and I. Laszlo. 1992. “Modeling Surface Solar Irradiance for Satellite

Applications on a Global Scale.” *Journal of Applied Meteorology* 31 (2) (February): 194–211. doi:10.1175/1520-0450(1992)031<0194:MSSIFS>2.0.CO;2.
Posselt, Rebekka, Richard Mueller, Reto Stöckli, and Jörg Trentmann. 2011. “Spatial and Temporal Homogeneity of Solar Surface Irradiance Across Satellite Generations.” *Remote Sensing* 3 (12) (May 20): 1029–1046. doi:10.3390/rs3051029.
Posselt, R., R. W. Mueller, R. Stöckli, and J. Trentmann. 2012. “Remote Sensing of Solar Surface Radiation for Climate Monitoring—the CM-SAF Retrieval in International Comparison.” *Remote Sensing of Environment* 118: 186–198.
Posselt, R., Richard Müller, Reto Stöckli, and Jörg Trentmann. 2011. “CM SAF Surface Radiation MVIRI Data Set 1.0 - Monthly Means / Daily Means / Hourly Means.” *Satellite Application Facility on Climate Monitoring (CM SAF)*.
Posselt, R., R. Müller, J. Trentmann, and R. Stöckli. 2011. “Meteosat (MVIRI) Solar Surface Irradiance and Effective Cloud Albedo Climate Data Sets.” *EUMETSAT Satellite Application Facility on Climate Monitoring, Validation Report* (1.1) (January 26): 1–51.
Reanalysis Intercomparison and Observations. 2012. “Comparison Table | Reanalysis Intercomparison and Observations.” *Reanalysis Intercomparison and Observations*. http://reanalyses.org/atmosphere/comparison-table.
Reda, Ibrahim, Tom Stoffel, and Daryl Myers. 2003. “A Method to Calibrate a Solar Pyranometer for Measuring Reference Diffuse Irradiance.” *Solar Energy* 74 (2) (February): 103–112. doi:10.1016/S0038-092X(03)00124-5.
Rienecker, Michele M., Max J. Suarez, Ronald Gelaro, Ricardo Todling, Julio Bacmeister, Emily Liu, Michael G. Bosilovich, et al. 2011. “MERRA: NASA’s Modern-Era Retrospective Analysis for Research and Applications.” *Journal of Climate* 24 (14) (July): 3624–3648. doi:10.1175/JCLI-D-11-00015.1.
Rigollier, Christelle, Mireille LefÈvre, and Lucien Wald. 2004. “The Method Heliosat-2 for Deriving Shortwave Solar Radiation from Satellite Images.” *Solar Energy* 77 (2): 159–169.
Satoh, Masaki. 2004. *Atmospheric Circulation Dynamics and Circulation Models*. 1st ed. Springer.
Sawaengphotkhai, P.C. 2009. “About FLASHFlux.” *National Aeronautics and Space Administration*. http://flashflux.larc.nasa.gov/common/php/FLASHFlux_About.php.
Scharmer, K., and Jürgen Greif. 2000. *The European solar radiation atlas. Vol. 1, Fundamentals and maps*. Paris: École des Mines.
Sieger, Rainer. 2012. “BSRN Toolbox.” *PangaWiki*. http://wiki.pangaea.de/wiki/BSRN_Toolbox.
SoDa: Solar Radiation Data. 2012. “SoDa - Times Series of Radiation Data for Registered Users.” *SoDa*. http://www.soda-is.com/eng/services/services_radiation_pay_eng.php.
Srivastava, G. P. 2009. *Surface Meteorological Instruments And Measurement Practices*. Atlantic Publishers & Dist.
Stackhouse, Paul W. 2011. “Surface Meteorology and Solar Energy (SSE) Release 6.0 Methodology.” *Atmospheric Science Data Center, National Aeronautics and Space Administration* 3.0 (April 19): 1–54. 2012.
Trentmann, Jörg, Richard Müller, Rainer Hollmann, and Martin Werscheck. 2012a. “AVHRR GAC Surface Radiation Products.” *EUMETSAT Satellite Application Facility on Climate Monitoring, Product User Manual* (1.1) (November 5): 1–16.
———. 2012b. “GAC Surface Radiation.” *EUMETSAT Satellite Application Facility on Climate Monitoring, Validation Report* 1.1 (November 5): 1–22.
Trentmann, Jörg, Christine Träger-Chatterjee, Richard Müller, R. Hollmann, and Martin

Werscheck. 2010. “Surface Radiation Products.” *EUMETSAT Satellite Application Facility on Climate Monitoring, Product User Manual* (2.1) (June 17): 1–52.

Trentmann, Jörg, Christine Träger-Chatterjee, Richard Müller, Rebekka Posselt, Reto Stöckli, R. Hollmann, and Martin Werscheck. 2012. “Meteosat (MVIRI) Solar Surface Irradiance and Effective Cloud Albedo Climate Data Sets.” *EUMETSAT Satellite Application Facility on Climate Monitoring, Product User Manual* (1.3) (April 24): 1–34.

Tsujikawa, Tatsuhiro. 2012. “Aria2 - The Next Generation Download Utility.” *Sourceforge*. http://aria2.sourceforge.net/.

United Nations. 2007. *Climate Change 2007: The Physical Science Basis*. 1 PAP/CDR. Intergovernmental Panel on Climate Change.

Uppala, S. M., P. W. KÅllberg, A. J. Simmons, U. Andrae, V. Da Costa Bechtold, M. Fiorino, J. K. Gibson, et al. 2005. “The ERA-40 Re-analysis.” *Quarterly Journal of the Royal Meteorological Society* 131 (612) (October): 2961–3012. doi:10.1256/qj.04.176.

US Department of Commerce, NOAA. 2008. “PSD/Climate Diagnostics Branch, Data: NCEP/NCAR Reanalysis.” http://www.esrl.noaa.gov/psd/data/gridded/data.ncep.reanalysis.surfaceflux.html.

U.S. Department of Energy, Office of Energy Efficiency and Renewable Energy, National Renewable Energy Laboratory. 2008. “National Solar Radiation Data Base.” *Renewable Resource Data Center*. http://rredc.nrel.gov/solar/old_data/nsrdb/1991-2005/tmy3/.

Warner, Thomas Tomkins. 2011. *Numerical Weather and Climate Prediction*. Cambridge University Press.

Wielicki, Bruce A., Bruce R. Barkstrom, Edwin F. Harrison, Robert B. Lee, G. Louis Smith, and John E. Cooper. 1996. “Clouds and the Earth’s Radiant Energy System (CERES): An Earth Observing System Experiment.” *Bulletin of the American Meteorological Society* 77 (5) (May): 853–868. doi:10.1175/1520-0477(1996)077<0853:CATERE>2.0.CO;2.

Wikimedia Commons. 2012a. “Pyrheliometer.” *Wikipedia, the Free Encyclopedia*. http://en.wikipedia.org/w/index.php?title=Pyrheliometer&oldid=508443425.

———. 2012b. “Pyranometer.” *Wikipedia, the Free Encyclopedia*. http://en.wikipedia.org/w/index.php?title=Pyranometer&oldid=505438986.

Wilks, Daniel S. 2005. *Statistical Methods in the Atmospheric Sciences: An Introduction*. 2nd revised ed. Academic Press.

World Radiation Monitoring Center – Baseline Surface Radiation Network. 2012a. “Project Background.” *Alfred Wegener Institute for Polar and Marine Research*. 2012. http://www.bsrn.awi.de/en/project/background/.

———. 2012b. “BSRN - World Radiation Monitoring Center Measurements.” http://www.bsrn.awi.de/en/data/measurements/.

———. 2012c. “BSRN - World Radiation Monitoring Center Data Retrieval via PANGAEA.” *Alfred Wegener Institute for Polar and Marine Research*. http://www.bsrn.awi.de/en/data/data_retrieval_via_pangaea/.

Zhang, Yuanchong, William B. Rossow, Andrew A. Lacis, Valdar Oinas, and Michael I. Mishchenko. 2004. “Calculation of radiative fluxes from the surface to top of atmosphere based on ISCCP and other global data sets: Refinements of the radiative transfer model and the input data.” *Journal of Geophysical Research* 109 (D19) (October 6): D19105. doi:10.1029/2003JD004457.

Appendix

7.1. Source code